

**Microfluidic Applications for the Study of Pancreatic Islets, Gradient Formation,
and Gas Diffusion**

By

Elizabeth Ferraz

B.S. University of Illinois at Chicago, Chicago, IL, 2010

THESIS

Submitted as partial fulfillment of the requirements for the degree
of Master of Science in Bioengineering in the Graduate College of
the University of Illinois at Chicago, 2015

Chicago, Illinois

Defense Committee:

David T. Eddington, Chair and Advisor

Yong Wong, Department of Surgery

Jun Cheng

This thesis is dedicated to Chris. You are my rock.

ACKNOWLEDGEMENTS

I would like to thank my husband, Chris, for supporting me every step of the way, having patience, and giving me daily encouragement. Many thanks to my parents, João and Edenilda, for instilling in me the desire to further my education, supporting me in my choices, and allowing me to live rent free for many years.

Thank you to David Eddington for being my research advisor and financially supporting me during my research. Thank you to Yong Wong for teaching me all I know about pancreatic islets and being part of my committee. Many thanks to Jun Cheng for being part of my committee and for being a wonderful professor.

Lastly, I would like to thank all of my labmates, past and present, for making coming to lab enjoyable. I will miss you all. I also thank all of the members in the Oberholzer lab for allowing me to use their microscope on a weekly basis and for always helping me. I also thank Arash Darbandi for being a wonderful undergraduate research assistant.

TABLE OF CONTENTS

Summary	1
Chapter 1: Fabrication of a multi-gradient device for liver zonation	2
1.1 Abstract	2
1.2 Introduction	2
1.3 Methods and materials	3
1.3.1 Device fabrication	7
1.3.1.1 Static gradient device	7
1.3.1.2 Dilution tree	8
1.3.1.3 Dilutions of dilutions	10
1.3.2 Gradient formation of static gradient device	12
1.3.2.1 Experimental setup	12
1.3.2.2 Analysis of gradient	12
1.3.2.3 Static gradient Comsol simulation	13
1.3.3 Gradient formation of dilution tree	13
1.3.3.1 Experimental setup	13
1.3.3.2 Analysis of gradient	13
1.3.4 Determining the channel resistance of dilutions of dilutions device	14
1.3.5 Experimental setup for dilutions of dilutions device	14
1.3.6 Comsol simulation of dilutions of dilutions device	15
1.4 Results	15
1.4.1 Static gradient device with FITC-dextran results	15
1.4.2 Comsol simulation of static gradient device results	16
1.4.3 Gradient of dilution tree results	18
1.4.4 Analysis of dilutions of dilutions device	18
1.4.5 Determining fluidic resistance	18
1.4.6 Comsol simulation of dilutions of dilutions device	19
1.5 Discussion	22
1.5.1 Static gradient device with FITC-dextran analysis	22
1.5.2 Comsol simulation of static gradient device	22
1.5.3 Gradient of dilution tree	23
1.5.4 Analysis of dilutions of dilutions device	23
1.5.5 Fluidic resistance analysis	25
1.5.6 Comsol simulation of dilutions of dilutions device	25
1.6 Future directions	26
1.7 Conclusions	27
1.8 References	27

Chapter 2: Islet perfusion with droplet generation for analysis with capillary electrophoresis	29
2.1 Abstract	29
2.2 Introduction	30
2.3 Methods and materials	35
2.3.1 Design of perfusion chamber	35
2.3.2 Fabrication of perfusion chamber	37
2.3.3 Computer simulation of perfusion chamber	39
2.3.4 Krebs Ringer buffer	39
2.3.5 Pancreatic islets isolation and culture	40
2.3.6 Incubation of islet cells in Fura-2AM	41
2.3.7 Perfusion chamber experimental setup	41
2.3.8 Design of droplet generator device	42
2.3.9 Fabrication of droplet generator	43
2.3.10 Experimental setup of droplet generator	45
2.3.11 Size and frequency of droplets	45
2.3.12 Capillary electrophoresis chip	46
2.3.13 Preparation of balanced salt solution and immunoassay buffer	47
2.3.14 Droplet analysis by capillary electrophoresis	48
2.3.15 Islet perfusion chamber mixer design and fabrication	49
2.3.16 Droplet collection for capillary electrophoresis	50
2.4 Results	51
2.4.1 Comsol simulation of perfusion chamber	51
2.4.2 Calcium response of islets with perfusion chamber	52
2.4.3 Droplet generator device	53
2.4.4 Calcium response with droplet generator device	54
2.4.5 Electropherogram with droplet generator device and CE chip	55
2.4.6 Results with islet perfusion chamber mixer device	55
2.5 Discussion	56
2.5.1 Comsol simulation of perfusion chamber	56
2.5.2 Calcium response in perfusion chamber	56
2.5.3 Droplet generator device	57
2.5.4 Calcium response with droplet generator	57
2.5.5 Droplet analysis with CE chip	58
2.5.6 Islet perfusion mixer device	58
2.6 Future directions	59
2.7 Conclusions	59
2.8 References	60
Chapter 3: Series of tubes – A novel technique using silicone tubing for oxygen sensitive experiments	62
3.1 Abstract	62
3.2 Introduction	62
3.3 Methods and materials	64

3.3.1	Types of tubing	64
3.3.2	Fabrication of 6-well insert	64
3.3.3	Design of oxygen perfusion chamber	66
3.3.4	Fabrication of oxygen perfusion chamber	67
3.3.5	Fabrication of PtOEPK	68
3.3.6	Calibration for tube analysis	68
3.3.7	Experimental setup for tube analysis	68
3.3.8	Calibration for 6-well insert	69
3.3.9	Experimental setup for 6-well insert	70
3.3.10	Calibration of perfusion chamber using PtEOPK	70
3.3.11	Experimental setup of perfusion chamber using PtEOPK	70
3.4	Results	71
3.4.1	Results of tube analysis	71
3.4.2	Results of 6-well insert	72
3.4.3	Results of perfusion chamber	73
3.5	Discussion	73
3.5.1	Tube analysis	73
3.5.2	6-well insert device	74
3.5.3	Perfusion chamber	74
3.6	Future directions	75
3.7	Conclusions	75
3.8	References	76

LIST OF FIGURES

Chapter 1

1.1	“Christmas tree” gradient generator	4
1.2	Examples of diffusion-based gradient generators	5
1.3	Schematic of static gradient device	8
1.4	Illustration of dilution tree	9
1.5	Iterations of dilutions of dilutions device	10-11
1.6	FITC-dextran gradient of static gradient device	16
1.7	FITC-dextran intensity	16
1.8	Comsol simulation of static gradient device	17
1.9	Simulation of 10 cell chambers dilutions of dilutions device	20
1.10	Simulation of 4 cell chamber dilution of dilution device	21

Chapter 2

2.1	Drawing of the islet transplantation process	31
2.2	Schematic of the 2nd phase of insulin release	32
2.3	Schematic of a CE system	34
2.4	Images of 5 μ L perfusion chamber	37
2.5	Droplet generator device	43
2.6	Example of the CE chip	48
2.7	Image of the islet perfusion chamber mixer device	50
2.8	Schematic of the droplet collection from fraction collection	51
2.9	Comsol simulation of flow within the 20 μ L and 5 μ L perfusion chamber	52
2.10	Ca ²⁺ response of 5 μ L perfusion chamber	53
2.11	Images of the droplet generator device	53-54
2.12	Ca ²⁺ response with droplet generator device	54
2.13	Electropherogram of insulin concentration with droplet generator	55
2.14	Three experiments of Ca ²⁺ response with perfusion chamber mixer device	56

Chapter 3

3.1	Schematic and images of 6-well insert	65
3.2	Schematic of oxygen perfusion chamber	67
3.3	Experimental setup for tube analysis with oxygen sensing probe	69
3.4	Oxygen concentration at different lengths and diameters of silicone and tygon tubing	71-72

LIST OF TABLES

Chapter 1

1.1	The length and fluidic resistance	19
-----	-----------------------------------	----

Chapter 3

3.1	List of tubing and dimensions	64
3.2	Oxygen concentration obtained from perfusion chamber	72

LIST OF ABBREVIATIONS

PDMS	polydimethylsiloxane
FITC	fluorescein isothiocyanate
DI	deionized
O ₂	oxygen
FOXY	fluorescent oxygen sensor (ruthenium based)
KRB	Krebs Ringer Buffer
EtOH	ethanol
Ca ⁺	calcium
Fura-2AM	fura-2 acetoxymethyl ester
FITC-insulin	fluorescein isothiocyanate insulin
Ab	anti-insulin antibodies
PFD	10:1 of perfluorodecalin and perfluorooctanol
HPFA	high purity perfluoroalkoxy alkane
fps	frames per second
CE	capillary electrophoresis
ddH ₂ O	double distilled water
HNO ₃	nitric acid
HF	hydrofluoric acid
BSS	balanced salt solution
BSA	bovine serum albumin
IB	immunoassay buffer
PMT	photomultiplier tube

B	bound FITC-insulin
F	free FITC-insulin
OD	outer diameter
IPA	isopropanol
PtOEPK	platinum(II) octaethylporphine ketone
PS	polystyrene
ID	inner diameter
N ₂	nitrogen
Si	silicon
DM	diabetes mellitus
T1	type 1 diabetes mellitus
T2	type 2 diabetes mellitus

SUMMARY

Microfluidic applications are essential for studying pancreatic islets for islet transplantation, gradient formation for liver function, and gas diffusion. In this research, we explore how microfluidics affects each of these areas. A microfluidic perfusion droplet device was design and fabricated to detect insulin levels of pancreatic islets. This device was designed to generate droplets and injected directly into a capillary electrophoresis chip where electropherograms of insulin levels are outputted. Next, a multi-gradient flow-based/diffusion-based device, called dilutions of dilutions, was designed, fabricated, and characterized. This device was designed to study the function of hepatocytes in different concentration gradients. In addition, a series of tubes were examined to evaluate the ability of using different lengths and diameters of gas permeable tubes to replace the need of costly specialty gas tanks.

Chapter 1: Dilutions of dilutions: Fabrication of a multi-gradient device for liver zonation

1.1 Abstract

Within the liver, hepatocytes reside in lobes, or zones. Little is known about how the zones interact and function with each other, other cell types, and oxygen concentrations. Chemical gradients *in vivo* play an important role in regulating zone functions; however, replicating the many gradients can be quite difficult. In this research, we design and fabricate a multi-gradient device for studying liver zonation called dilutions of dilutions. By combining two existing techniques of gradient formation, flow-based and diffusion-based gradient generators, the dilutions of dilutions device is able to generate a variety of gradients on-chip. Hepatocytes are sensitive to mechanical forces, which can arise from flow-based gradient generators. To bypass this issue, the flow-based gradient generator is used to mix and dilute chemical reagents, which is then combined with multiple diffusion-based gradient generators to create a static gradient cell culture chamber. The dilutions of dilutions device will permit us to evaluate how hepatocytes function under each type of chemical gradients. This device can then be modified to treat each cell culture chamber with different oxygen concentrations.

1.2 Introduction

Microfluidics is an essential tool in recreating cellular microenvironments for studying growth, migration, and chemical/hormonal interactions. Understanding the fundamental processes of the cellular mechanisms in these environments can provide better understanding to immune response, cellular functionality, cancer metastasis, and wound healing leading to improving and expanding current treatment methods. The most common type of these microenvironments *in vivo* is chemical gradients and can be difficult to produce *in vitro*.

The first techniques to recreate gradients (Boyden 1962, Zicha 1991, Zigmond 1979) were unpredictable and difficult to characterize. Other gradient techniques were limited to time, dissipating within hours and limiting investigations (Chen 1998, Foxman 1997). To overcome these issues, microfluidics devices have been developed to create precise and controllable gradients of soluble and insoluble factors. The gradients produced by these devices are reproducible and quantifiable, generating a variety of shapes (Cooksey 2009, Abhyankar 2006, Dertinger 2002). In this research, we combine two types of gradient generators: flow- and diffusion-based.

Flow-based gradient generators, form gradients within a region via convection through laminar flow. Laminar flow is described as streams of fluid mixing together by diffusion without turbulent disturbances (Whitesides 2001). The simplest type of flow-based gradient generator is a Y, or T, -shaped channel where two laminar fluids diffuse together (Schilling 2002, Hatch 2004). This type of gradient generator creates a step-like gradient immediately after the junction point of the inlets and a sigmoidal gradient further downstream (Schilling 2002). Unfortunately, the Y-shaped channel is limited to creating a sigmoidal shape based on the flow rates used. Another type of flow-based generator is a “Christmas tree” shaped device (Jeon 2000) that is able to create a variety of gradient profiles. This device is made of a network of bifurcated channels where different concentrations are infused into the inlets then split, mixed, and recombined through the channels, Figure 1.1. The streams recombine at the outlet creating a laminar flow gradient. Each “stem,” or stream, is composed of its own specialized concentration. As with the T-shaped gradient generator, the gradient profile for the “Christmas tree” is dependent upon the flow rate.

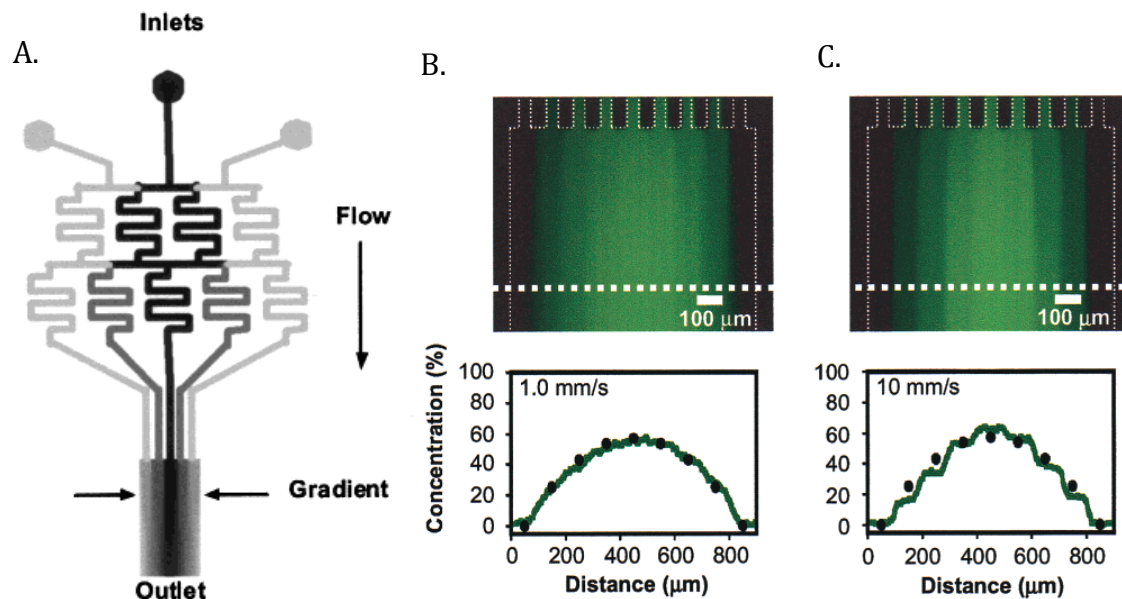


Figure 1.1. “Christmas tree” gradient generator. A) Schematic of flow-based gradient generator. Gradient profiles at the outlet of the “Christmas tree” device with a flow rate of 1 mm/s (B) and 10 mm/s (C). (Reprinted from Jeon 2000)

Cells can easily be added to the outlet channels of the “Christmas tree” and T-shape devices through a secondary outlet channel (Jeon 2002) or through the outlet itself (Schilling 2002), respectively. The cells are then subjected to the laminar flow of the devices. Unfortunately, flow-based generator can have an unfavorable effect on cell response and interactions. Laminar flow can cause shear stress on certain cell lines, specifically endothelial cells whereby altering their physiological response (Fisher 2001). In addition, important secreted factors can be easily washed away (Yu 2005). This can affect the cell itself, or affect cell-cell interactions, hindering the results obtained. The laminar flow can also persuade the migration of the cells within the cell culture area (Walker 2005).

Diffusion-based gradient generators formulate gradients via diffusion transport in a convection-free area. The gradient forms in a desired area as molecules diffuse from a “source” to a “sink” (Abhyankar 2006, Shamloo 2008, Keenan 2006). To create the

gradients, high fluidic resistances in microchannels, or microjets, (Shamloo 2008, Keenan 2006) or porous membranes (Abhyankar 2006, Kim 2009) are typically used, Figure 1.2. Since there are physical barriers preventing convection flow, the concentration gradient occurs gradually over time until a steady state is achieved. The higher the fluidic resistance, the longer it takes for the gradient to form. The microjets are low in height, narrow width, and long, creating a high fluidic resistance while minimizing convection flow. By flowing at the same rates in both the source and sink channels, the pressure at both ends of the microjets are balanced, creating a sustained flow across the area of interest, usually the cell culture chamber. In this thesis, we call these types of convection-free devices, static gradient devices.

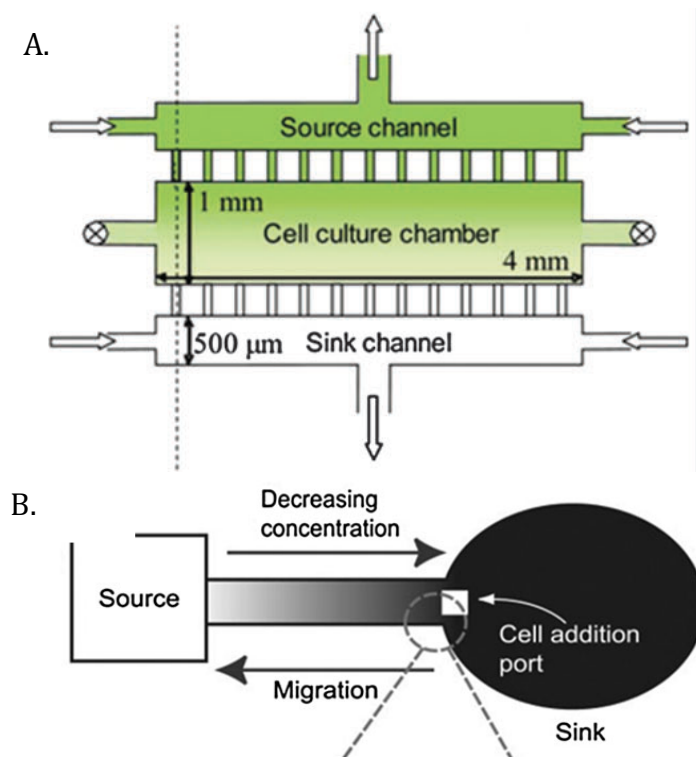


Figure 1.2. Examples of diffusion-based gradient generators. A) Schematic of gradient generator developed by Shamloo *et al.* The gradient forming area is lies in between the source and sink channels, separated by microjets. B) Schematic of gradient generator developed by Abhyankar *et al.* The gradient forming area is separated from the sink and source regions by a porous membrane.

In the static gradient devices, the cells are added to the devices via a port, or inlet, connected to the culture chamber. Due to the nature of the devices, the cells are exposed to static flow, eliminating the formation of shear stress on the cells. The shape of the concentration gradient is dependent on the molecules of the reagents and the overall structure of the gradient formation area. Due to the static gradient, the accumulation of paracrine and autocrine factors is possible, giving new understanding of cell-cell interaction, migration, and cell response. By providing constant flow to the channels, the gradient is continuously replenished allowing for constant temporal control.

With combining these technologies, flow-based and diffusion-based gradient generators, we create a multi-diffusion-based gradient generator, dilutions of dilutions, to study how hepatocytes affect the functionality of the each liver lobe. Blood enriched oxygen, from the hepatic artery, determines the structure of the liver plate within the liver lobule. The function of the hepatocytes differ depending upon their position, or zones, along the liver plate (Katz 1977). Gradients of hormones and oxygen (O_2) strongly affect liver zonation but little is known on how the gradients and zones interact with each other. Microfluidic technology allows for the precise control of the hepatocytes by mimicking the environmental factors the cells experience *in vivo*. By creating the dilutions of dilutions device, an array of bioreactors with static gradient diffusion of different concentrations will expose hepatocytes to varying chemical factors. A flow-based gradient generator, similar to the “Christmas tree”, or dilution tree, will create a dilution of two chemicals. The dilution will feed into multiple static gradient generators, each with their own gradient profile. Hepatocytes and fibroblasts, for supporting liver function, will be seeded into the cell culture chamber of the static gradient generators allowing us

to understand function of liver zonation and how they are affected by drug toxicity and industrial chemicals.

1.3 Methods and materials

1.3.1 *Device Fabrication*

In order to develop the dilutions of dilutions device, each dilution method, dilution tree and static gradient, were individually fabricated and tested to ensure a gradient could be achieved. Once the gradients were established individually, the two methods were then combined.

1.3.1.1 Static gradient device

The static gradient device, Figure 1.3, is fabricated using a two-step photolithography process. Each layer was added in a stepwise fashion onto a 3” silicone wafer using SU-8 photoresist (Microchem). The first layer is comprised of two columns of 170 rows, or microjets. The rows are 5 μm wide by 600 μm long. The gap between the cell chamber and the source and sink channels are 400 μm . The 200 μm extension of the 5 μm channels are in place to assure in proper alignment of the second layer. The first layer of the static gradient master was made by spinning SU-8 2005 with a thickness of 5 μm onto a silicon wafer. The wafer was first dehydration at 120° C for 20 min. After cooling to room temperature, the wafer was place unto a spin coater (Laurell) where SU-8 2005 was added. The wafer was then spun at 500 rpm for 10 s followed by 3000 rpm for 30 s and then baked at 95° C for 2 min. Upon cooling to room temperature, the wafer was placed unto a μPG (Heidleberg Instruments) where the first layer can be exposed. When exposure was completed, the wafer was baked for 3 min at 95° C. The second layer, which consisted of the cell culture chamber, 1 mm wide by 4 mm long, the sink channel and the source channel, both start at 200 μm wide and increase to 400 μm , were

printed onto a mylar photomask (Fineline). For the second layer, SU-8 2150 was spun at 500 rpm for 10 s followed by 2000 rpm for 30 s to obtain a total height of 205 μm on the wafer. This layer was baked at 65° C for 6 min and 95° C for 45 min. The photomask was aligned to the first layer and exposed to UV light to 300 mJ/cm^2 energy. Afterwards, the wafer was baked at 65° C for 5 min and 95° C for 15 min. The entire wafer was then developed to remove any unexposed features for 20 min, producing the master of the design.

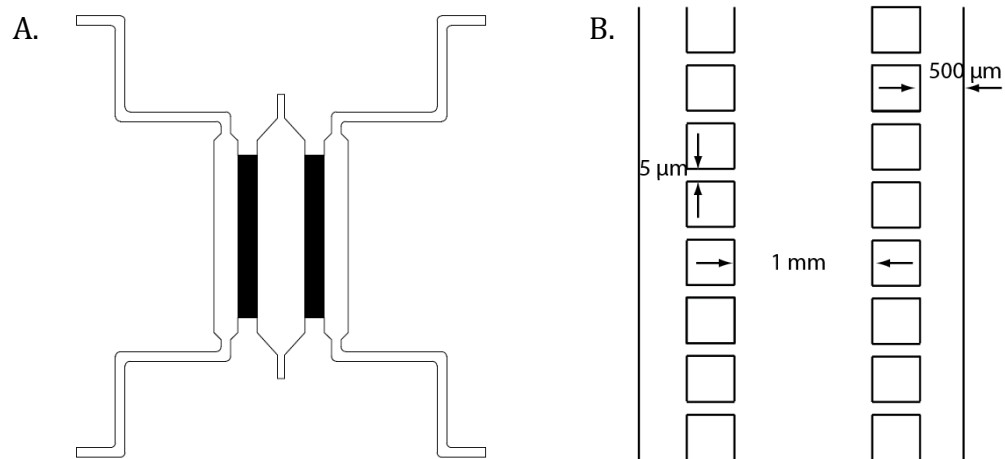


Figure 1.3. A) Schematic of static gradient device. B) Zoom in area of the cell culture chamber with dimensions.

After development, polydimethylsiloxane (PDMS) was premixed at a 10:1 ratio of polymer base to curing agent, degassed, and then cast onto the silicon wafer design. PDMS was cured at 85° C for 1.5 hrs, slowly removed, and 14 gauge holes were punched into the inlets and outlets for tubing insertion. The PDMS was cleaned with Scotch tape (3M) to remove any debris and bonded to a pre-cleaned 25 x 75 mm glass slide using a corona plasma treater (Electro-Technic Products, Inc.).

1.3.1.2 Dilution Tree

Figure 1.4 shows the design of the dilution tree used to validate the gradient mixing process. The channels had a width of the 100 μm and a depth of 200 μm . Each inlet divided into multiple channels and combined into a 1 mm wide channel. As previously mentioned, the device was fabricated using photolithography. First a 3'' silicon wafer underwent a dehydration bake. To get the 200 μm depth, SU-8 2150 was spun onto a 3'' silicon wafer at 500 rpm for 10 s followed by 2000 rpm for 30 s. The wafer was then baked at 65° C for 6 minutes and 95° C for 45 minutes. This was then exposed to UV light through a mylar photomask of the dilution tree design to 300 mJ/cm^2 . After exposure, the wafer was baked at 65° C for 5 minutes and 95° C for 15 minutes. It was then developed to uncover the design.

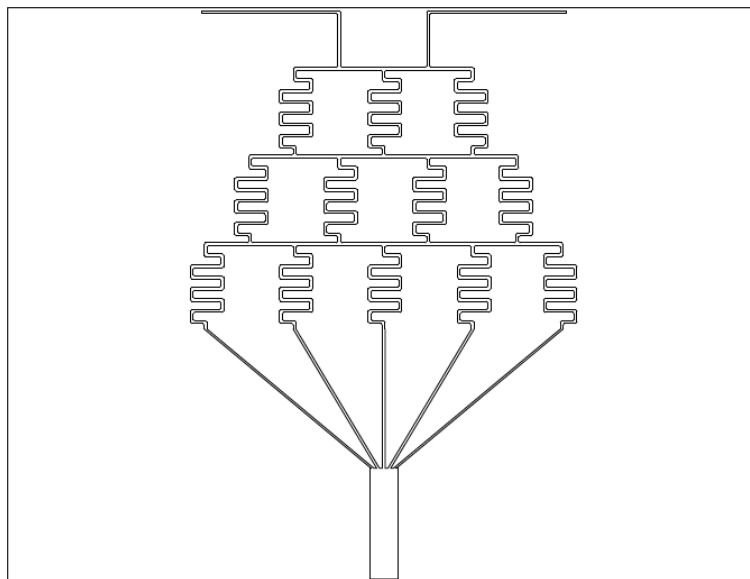


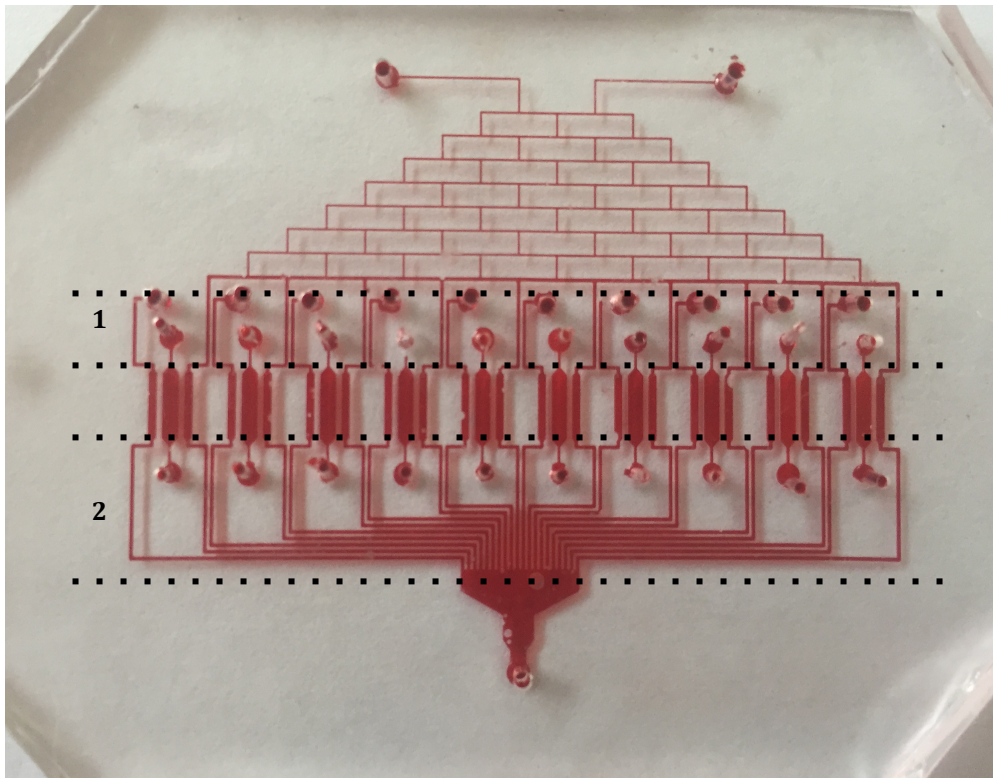
Figure 1.4. Illustration of the design of the dilution tree used to validate mixing.

As previously described, PDMS was mixed, cast, and cured onto the master. 14 gauge holes were punched into each inlet and outlet. The PDMS was bonded to a 50 x 75 mm glass slide with a corona plasma treater.

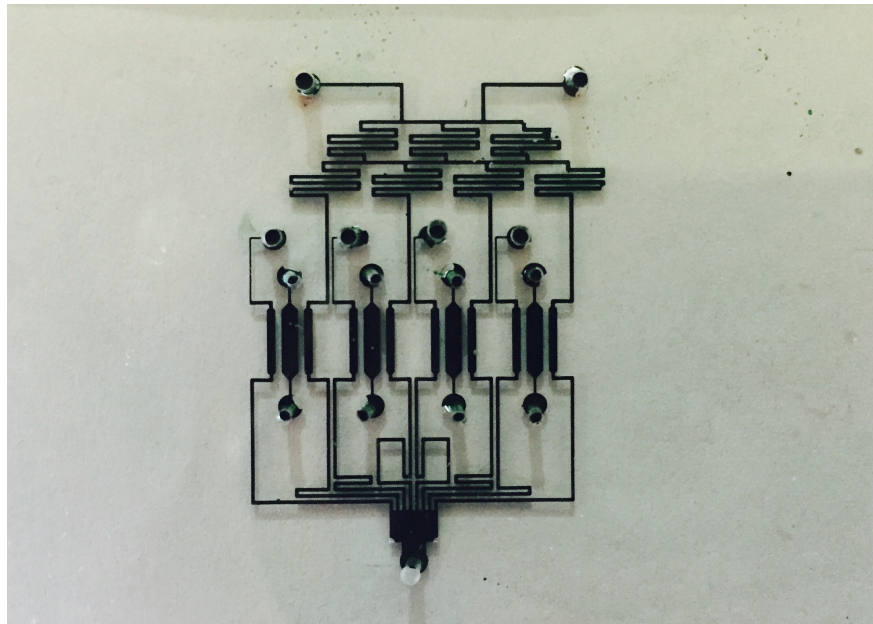
1.3.1.3 Dilutions of dilutions

The dilutions of dilutions device was designed by combining the static gradient and dilution tree designs, Figure 1.5a. The first half of the dilutions of dilutions has similar features of the dilution tree. Instead of combining to a 1 mm channel, each “dilution stem” connects to a source channel of a static gradient. For each “stem,” there is a static gradient chamber, 2 microjet rows, and a sink channel. Each one has the same dimensions as previously described for the static gradient device. The sink channels and the source channels from the dilution tree were combined to a 1 mm channel.

A.



B.



C.

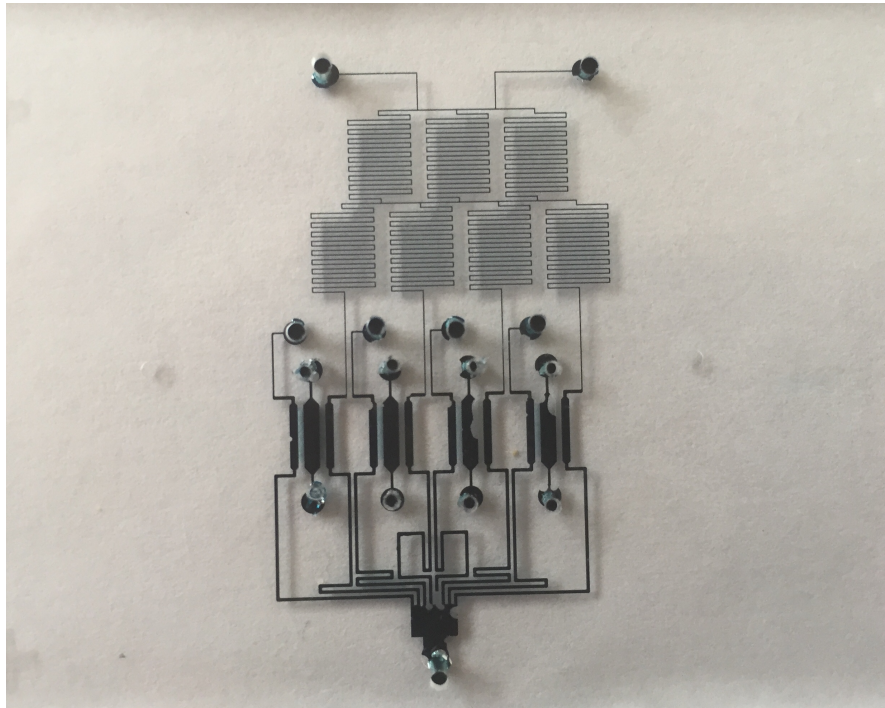


Figure 1.5. Different iterations of the dilutions of dilutions device. A) Initial design of the dilutions of dilutions device. Each “stem” goes from the dilution tree to the source channel of the static gradient device. After the cell chamber the sink and source outlet channels connect to an outlet. The fluidic resistance of the channels in section 1 and 2 were determined as discussed later. B) Second iteration with less static culture chambers C) Third iteration with longer “leaves” for the dilution tree to allow for better mixing of reagents.

The master was fabricated using the same techniques as the static gradient device but UV exposing the photoresist with the dilutions of dilutions photomask. After

development of the master, PDMS was cast, cured, and removed to allow hole punching of the inlets and outlets. The outlet and inlets of the dilution tree and sink channels were hole punched at 13 gauges. A 17 gauge hole was punched into the inlet and outlet of the cell culture chamber. The PDMS was then bonded to a 50 x 75 mm glass slide with a corona plasma treater.

1.3.2 Gradient formation of static gradient device

1.3.2.1 Experimental setup

Prior to each experiment, the static gradient device was perfused with ethanol to wet the channel surface. After 15 minutes, the device was rinse with DI water, ensuring to remove all bubbles including within the microjets. The cell chamber was then plugged at the inlets and outlets. A pipette tip was cut from the top and used as a funnel at the inlets of the source and sink channel. A syringe pump (Chemyx) capable of withdrawing was setup with two 1 mL syringes and tubing. The tubing was connected to the outlets of the source and sink channel. At the source channel, 5 μ M of FITC-dextran, which has similar molecular weight and diffusivity of VEGF, was put into its pipette tip. In the sink channel, DI water was placed into its pipette tip. The syringe pump was then set at a flow rate of 20 nL/min and left running for 3 hours. The microscope filter cube was set to FITC and data images were taken every 2 minutes using Metamorph software.

1.3.2.2 Analysis of gradient

Images of the gradient were analyzed using Image J. A line scan across the center of the chamber, from source channel to sink channel, was made. A histogram of the fluorescent intensity along the line was generated and evaluated.

For calibration, images of the source channel were taken. Using Image J, the intensity value of the fluorescence within the channel was determined and average out. Using this value, the intensity values from the line scan were normalized.

1.3.2.3 Static gradient Comsol simulation

A simulation of the static chamber was performed to confirm gradient formation. Two *Physics* models were used for the simulation: laminar flow and transport of diluted species. An AutoCAD file of the design was imported into the software. The 2D simulation module was selected. For the laminar flow the inlet and outlet channels were selected and set to 101325 Pa and -20 nL/min, respectively. The flow was set at a negative value to simulate the fluid being pulled through the device. For transport of diluted species, each inlet was set to different concentration values of 0 and 1 mol/m³. The outlet channels were set to outflow. The fluid flow values were set to the following: density – 1542 kg/m³, viscosity – 0.1 Pa•s, and diffusion coefficient – 9.4 cm²/s. Once the simulation ran with all the correct settings and values, the concentration results were displayed. A line was drawn across the chamber and a graph of the concentration created.

1.3.3. Gradient formation of dilution tree

1.3.3.1. Experimental setup

As previously described, each device was primed with ethanol and rinsed with water. Afterwards pipette tips, as previously described, were placed at the two inlet channels. Red and blue food dye was placed into each tip, respectively. The outlet port of the device was connected to a syringe pump. The syringe pump was set at a withdrawing velocity of 10 µL/min.

1.3.3.2 Analysis of gradient

The outlet channel of the dilution tree was observed for a gradient of the two dyes. The device ran for 1 hour, after which a gradient had formed and an image was taken.

1.3.4. Determining the channel resistance of dilutions of dilutions device

The resistance of each channel of the dilutions of dilutions device was determined in order to better understand flow dynamic within the channels. The following equation was used to determine the fluidic resistance, R , of each microchannel

$$R = \frac{12\mu L}{wh^3} \quad (1.1)$$

where w is the channel width, h is the channel height, μ is fluid viscosity (water in this case), and L is the channel length. The height and width used for this analysis were 250 and 200 μm , respectively. The length of each channel was determined from the end of the dilution tree split to just before the static gradient, marked 1 in Figure 1.5. In addition, the resistance after each static chamber was determined marked 2 in Figure 1.5. After the resistance was determined for each channel, the smallest channel resistance was chosen and the dimensions of the other channels in that set, either section 1 or 2, were adjusted to attain the desired resistance.

The fluidic resistance of the channels was determined for all iterations of the dilutions of dilutions device.

1.3.5 Experimental setup for dilution of dilutions device

The dilutions of dilutions device was setup in a similar manner to the static gradient and dilution tree devices. Each device was conditioned with ethanol and DI water. The device was observed under the microscope and bubbles were removed if necessary. Pipette tips were placed at the inlets of the sink and tree channels. 20 μM FITC-dextran was put into one of the tree inlets. In the other tree channel inlet and sink

channels, DI water was deposited. The outlet of the device was connected to a syringe pump capable of withdrawing. The flow rate of the device changed over the course of the project to determine which rate worked the most efficiently.

1.3.6 Comsol simulation of dilutions of dilutions device

In a similar manner to the simulation of the static chamber device, a simulation of the dilutions of dilutions device was performed. The *Physics* tools selected for simulation were the same as the static chamber. Each of the inlet channels were set to atmospheric pressure, and the outlet was set to a negative flow. One inlet channel of the dilution tree and the sink channels were set to a concentration of 0 mol/m^3 . The other inlet channel of the dilution tree was set 1 mol/m^3 . The outlet channel was set to outflow. Once the simulation was performed, a line graph of each chamber was generated.

1.4 Results

1.4.1 Static gradient with FITC-dextran results

As described the analysis of the static chamber was performed. The results in Figure 1.6 show the gradient formation of the static microfluidic chamber at a 20 nl/min flow rate. A linescan shows the normalized intensity of the center of the chamber, Figure 1.7.

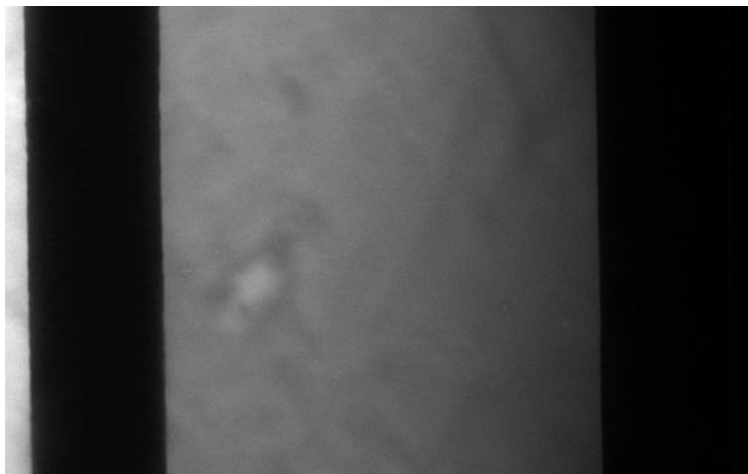


Figure 1.6. FITC-dextran gradient of static chamber after 20 minutes of equilibration.

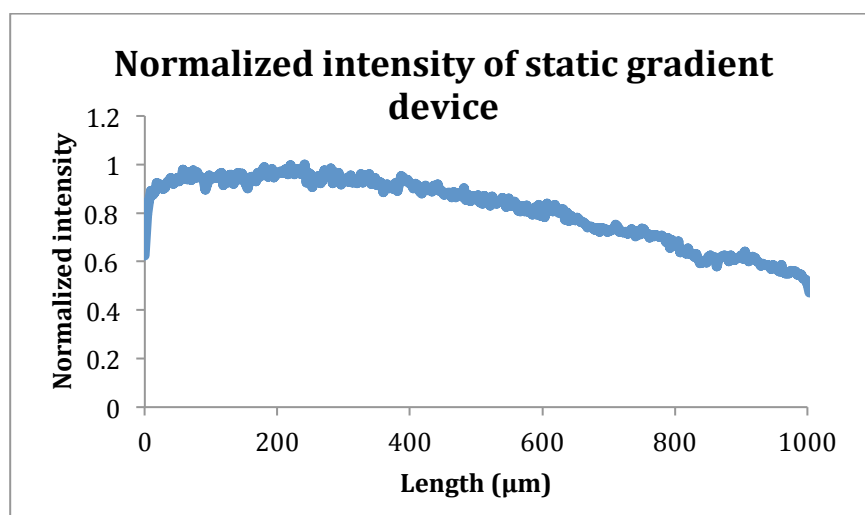


Figure 1.7. FITC-dextran intensity gradient across the cell chamber of the static gradient device after 20 minutes of equilibration. N=2.

1.4.2 *Comsol simulation of static gradient device results*

A simulation of the static gradient device was performed and the results are shown in Figure 1.8. With a 20 nL/min flow rate a gradient was able to form.

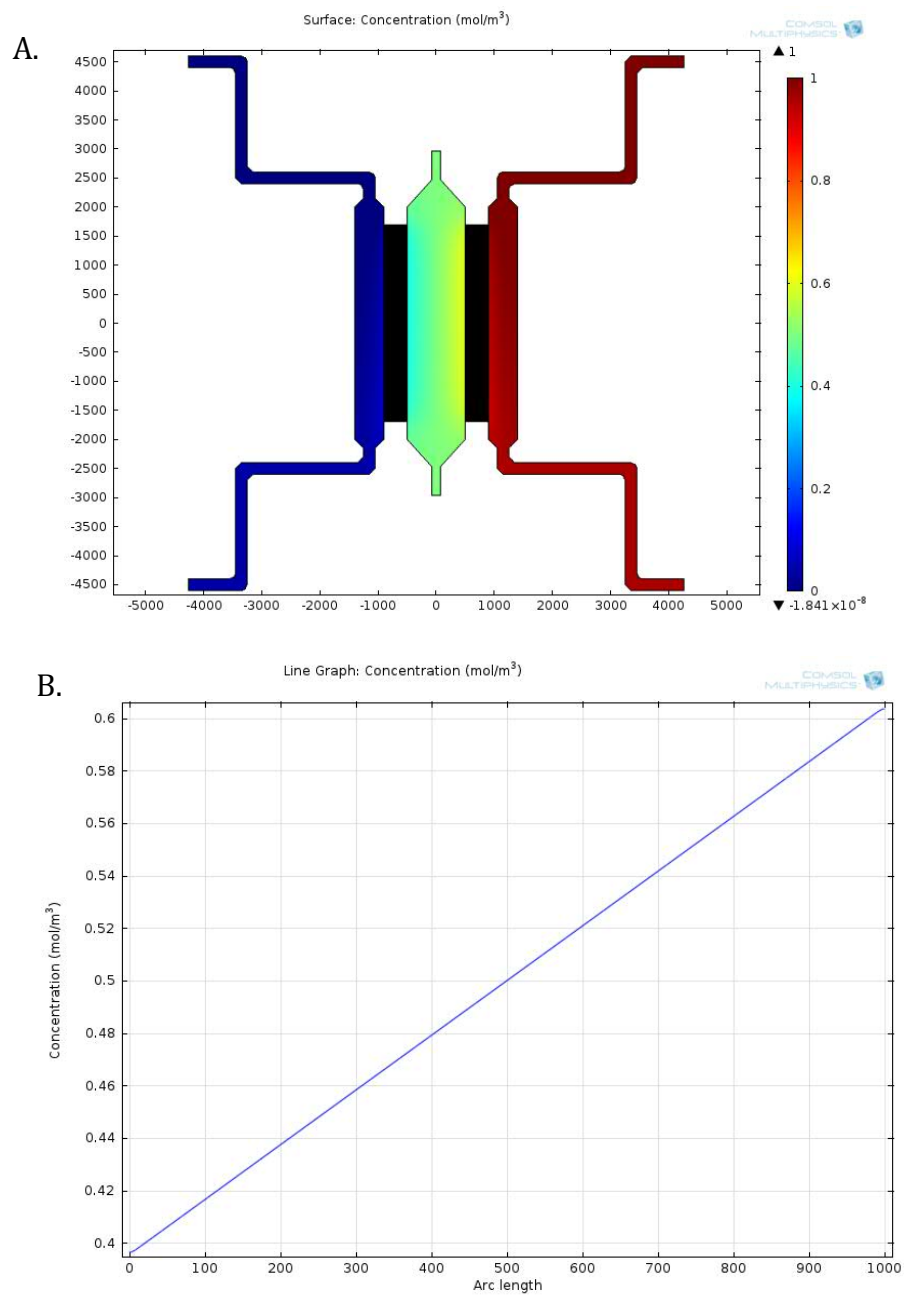


Figure 1.8. Comsol simulation of static gradient device. A) Concentration gradient generated in the cell chamber at a perfusion of 20 nL/min. Red is the source channel and blue is the sink channel. B) Line graph of the gradient in the cell chamber. The gradient ranges from 37% to 63%.

1.4.3 Gradient of dilution tree results

A simple dilution tree shown in Figure 1.4 was perfused with blue and red food dyes, not shown, to show the mixing within the tree. We were able to observe the formation of the gradient within the tree and validate a gradient.

1.4.4 Analysis of dilutions of dilutions

Due to the complexity of the dilutions of dilutions design, results of the FITC-dextran experiments were not obtained. The design went through many different iterations as shown in Figure 1.5 and discussed later.

1.4.5 Determining fluidic resistance

The resistance of each channel, 1-20 of Figure 1.5a, was determined. The largest resistance for the section 1 was determined to be $7.19 \times 10^{10} \text{ kg}\cdot\text{s}^{-1}\cdot\text{m}^{-4}$. The smallest resistance of section 2 was determined to be $6.85 \times 10^{10} \text{ kg}\cdot\text{s}^{-1}\cdot\text{m}^{-4}$.

Section 1-Before static gradient			Section 2-After static gradient to end		
Channel	Total Length (μm)	Fluidic Resistance (kg•s ⁻¹ •m ⁻⁴)	Channel	Total Length (μm)	Fluidic Resistance (kg•s ⁻¹ •m ⁻⁴)
1	5470	4.11E+10	1	30530.6104	2.29E+11
2	9564	7.19E+10	2	26230.6104	1.97E+11
3	5470	4.11E+10	3	26230.6104	1.97E+11
4	9564	7.19E+10	4	21930.6104	1.65E+11
5	5470	4.11E+10	5	21930.6104	1.65E+11
6	9564	7.19E+10	6	17630.6104	1.32E+11
7	5470	4.11E+10	7	17630.6104	1.32E+11
8	9564	7.19E+10	8	13330.6104	1.00E+11
9	5470	4.11E+10	9	13330.6104	1.00E+11
10	9564	7.19E+10	10	9116.6104	6.85E+10
11	5470	4.11E+10	11	9116.6104	6.85E+10
12	9564	7.19E+10	12	13330.6104	1.00E+11
13	5470	4.11E+10	13	13330.6104	1.00E+11
14	9564	7.19E+10	14	17630.6104	1.32E+11
15	5470	4.11E+10	15	17630.6104	1.32E+11
16	9564	7.19E+10	16	21930.6104	1.65E+11
17	5470	4.11E+10	17	21930.6104	1.65E+11
18	9564	7.19E+10	18	26230.6104	1.97E+11
19	5470	4.11E+10	19	26230.6104	1.97E+11
20	9564	7.19E+10	20	30530.6104	2.29E+11

Table 1.1. The length and fluidic resistance of channels 1-20 of section 1 and 2.

In a similar manner, the resistance of channels 1 and 8 from section 2 of Figure 1.5b was determined to be $4.76 \times 10^{11} \text{ kg}\cdot\text{s}^{-1}\cdot\text{m}^{-4}$. For each channel, 2-7, the length was adjusted to be equivalent to channels 1 and 8. Once this was done all channels of section 2 had the same resistance.

1.4.6 Comsol simulation of dilutions of dilutions

A simulation of dilutions of dilutions device similar to Figure 1.5a was obtained, Figure 1.9. In this simulation, “squiggles” were added to provide better mixing for the 0 and 1 mol/m³. Channels of section 1 and 2 were adjusted to obtain the same resistance for each section. The fluid flow was withdrawn from the device at a flow rate of 10 μL/min.

In addition, a simulation of Figure 1.5b was obtained, Figure 1.10. The velocity rate was set to $10 \mu\text{L}/\text{min}$. A gradient in each chamber formed, Figure 1.10b.

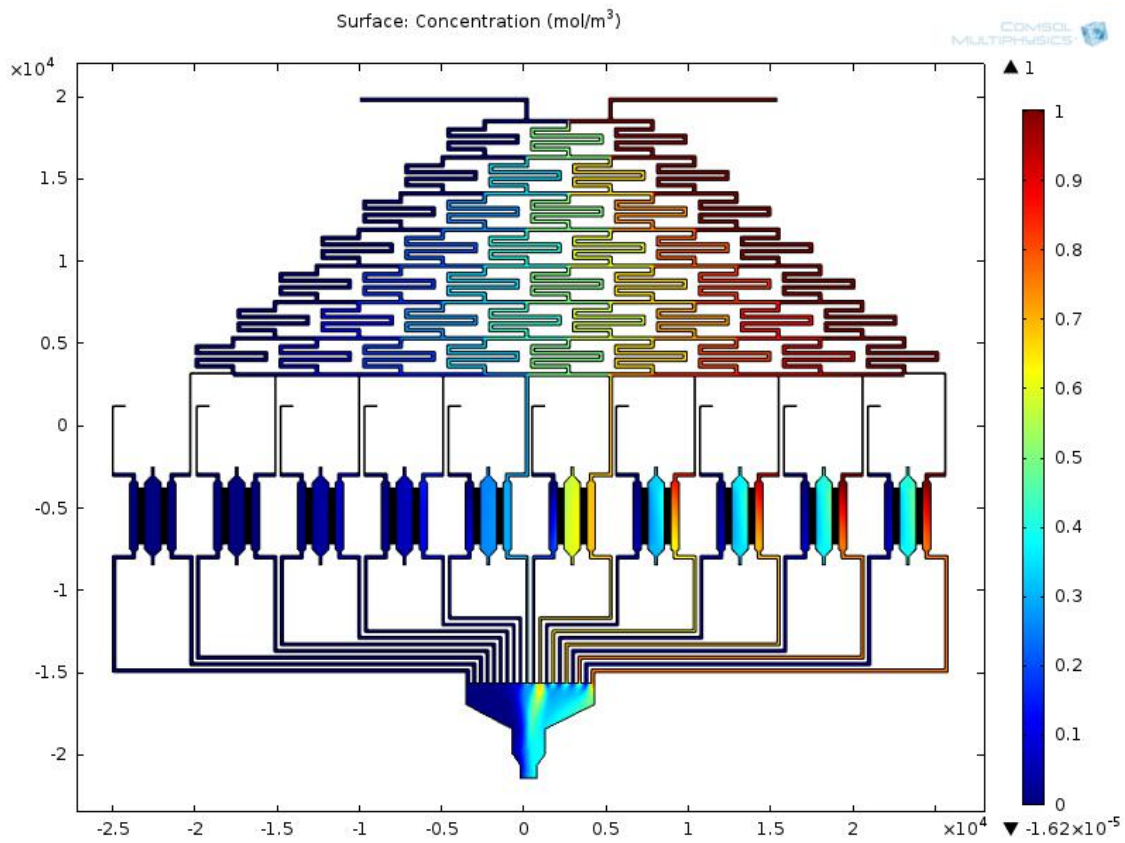


Figure 1.9. Simulation of 10 cell chambers dilutions of dilutions device at a withdraw flow rate of $10 \mu\text{L}/\text{min}$. Surface concentration where red and blue represent 1 and $0 \text{ mol}/\text{m}^3$, respectively.

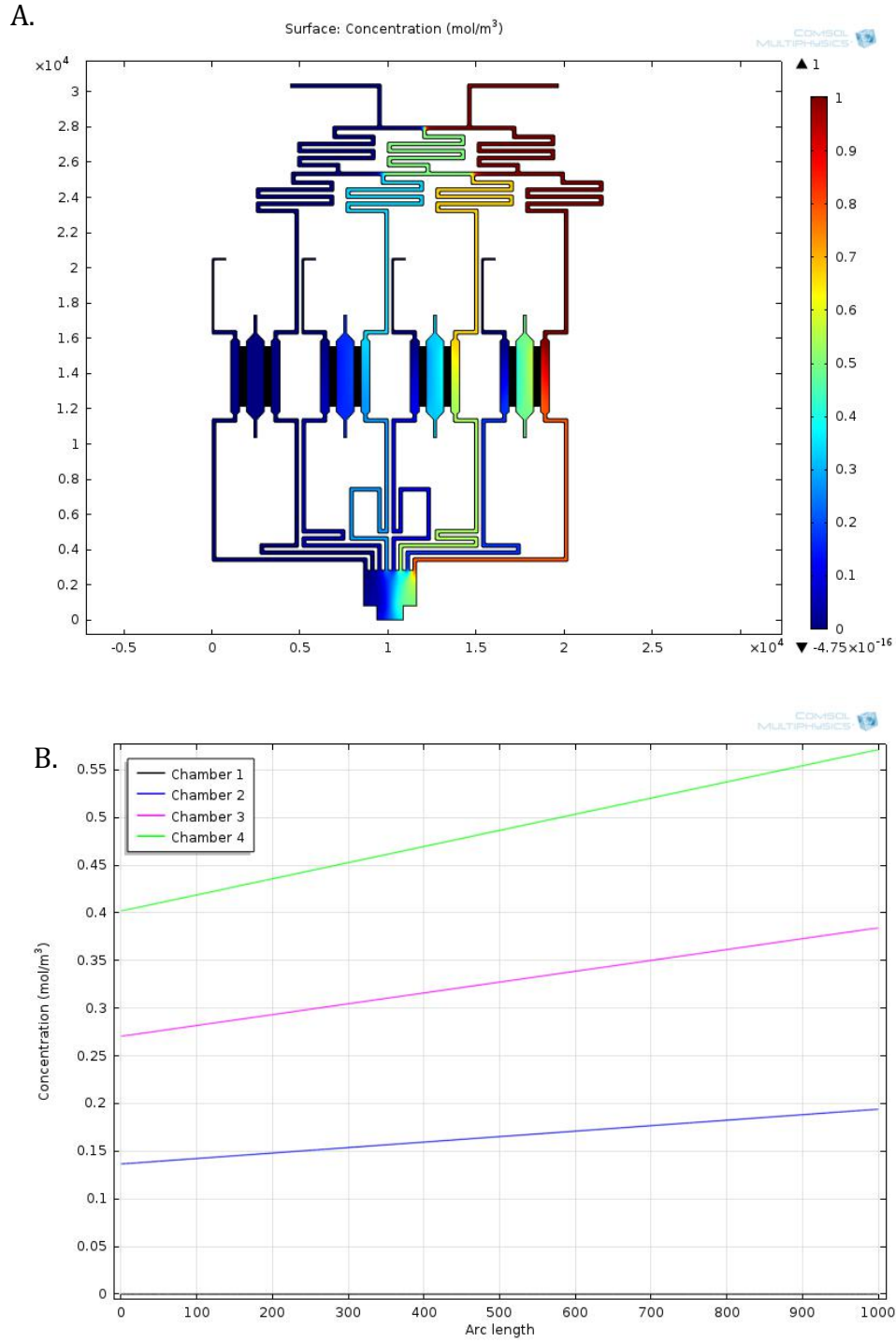


Figure 1.10. Simulation of 4 cell chamber dilution of dilution device. Same design as Figure 1.5b. A) Gradient formation in tree and static chamber. Red and blue represent 0 and 1 mol/m³, respectively. B) Line graph of gradient in cell chambers 1-4 (left to right).

1.5 Discussion

1.5.1 *Static gradient with FITC-dextran analysis*

The results in the cell culture chamber confirmed the formation of a gradient using 5 μ M FITC-dextran. However, the results of the gradient are much higher than published in Shamloo (2008). Shamloo showed that the gradient formed with a minimum and maximum concentration of 37% and 63%, respectively. Our results show that the minimum and maximum concentration is 55% and 85%, respectively. Shamloo's results have a concentration gradient of 26% while our results show a concentration gradient of 30%. Our gradient is within this range of 26%, demonstrating that we were able to successfully obtain a concentration gradient similar to Shamloo. Our concentration gradient may be higher due to the higher flow rate used during our experiments. Shamloo used a flow rate of 8 nL/min, while we used a flow rate of 20 nL/min. The increase flow rate would cause a higher concentration of FITC-dextran to diffuse into the chamber, thus increasing the gradient. We suspect that if a flow rate of 8 nL/min was used, we would obtain a gradient similar to Shamloo's. The gradient may also be higher due to a higher concentration of FITC-dextran. Perhaps the 5 μ M FITC-dextran used was miscalculated and a much higher concentration was used. It may be beneficial to reevaluate this experiment with new 5 μ M FITC-dextran, to re-verify the results.

In addition, our gradient was able to stay stable for at least 4 hours, the length of our experiment. We suspect that if the device was left to run longer that the static gradient would remain for much longer.

1.5.2 *Comsol simulation of static gradient device*

To further validate our static gradient device, we used Comsol to simulate the gradient formation. In our simulation, we obtained a gradient with a minimum and

maximum concentration of 37% and 63%, respectively. These results are identical to the simulation and experimental results obtained by Shamloo. This confirms that the static gradient device was designed to generate the desired concentration gradient.

1.5.3 Gradient of dilution tree

A dilution tree device was developed to understand the flow dynamics of the dilution tree. Jeon (2000) first developed the dilution tree device and showed that with different flow rates, a variety of gradient profiles can be developed. Since we were mainly interested in determining if the dilution tree would still function by withdrawing from the outlet, we developed a simple dilution tree pictured in Figure 1.4. Although not shown, we were able to visually observe a gradient formation with red and blue dye. This confirmed that the dilution tree would still function as expected via withdrawal.

1.5.4 Analysis of dilutions of dilutions

The first dilutions of dilutions device developed is pictured in Figure 1.5a. In performing the first fluorescent experiment, it was quickly determined that a gradient was not forming. The FITC-dextran and water did not diffuse and split into the branches as expected. The FITC-dextran would diffuse across the entire tree and into the water well. When the withdrawing rate was increased 10 fold, the FITC-dextran would diffuse and mix across a small section of the tree, not all of the branches. The flow would continue into the source channels of the static gradient portion of the device. However, due to the flow rate, the FITC-dextran could not diffuse into the cell culture chamber of the static gradient device. In order for the fluorescent to diffuse into the chamber via the microjets, the flow rates must be slow enough to allow for the diffusion. In order to reduce the flow rate and have mixing across the entire dilution tree, the fluidic resistance within the channels were calculated, discussed in the next section.

Once the fluidic resistance was calculated, the dilutions of dilutions device was redesigned to create the same resistance across all the channels. However, we still experienced problems in creating a gradient in the tree and cell culture chamber. Again, the fluorescence would only diffuse across a few channels and branches. Also a gradient was not observed in any of the 10 cell culture chambers. Squiggles in the dilution tree were added to help with mixing, Figure 1.9. Unfortunately, the squiggles did not improve the diffusion mixing across the entire tree. It did help with mixing the fluorescence and water in some of the branches.

After several attempts of redesigning the 10 chamber dilutions of dilutions device, it was decided to reduce the device to 4 chambers, Figure 1.5b. This would allow us to evaluate the dilution tree much easier. In addition to reducing the device to 4 chambers, the fluidic resistances at the outlet, after the cell culture chambers, were made equal by making the length of each channel equal. For the inlet channels, the sink channels were adjusted so that the fluidic resistances were equal by reducing the channel width to 50 μm . Once all the channels were adjusted, the fluorescence experiment was reevaluated. With the reduced chambers, it was observed the fluorescence was able to diffuse and mix better within the dilution tree. However, fluorescence was not able to diffuse into the cell culture chamber at the flow rate of 10 $\mu\text{L}/\text{min}$. The flow rate was reduced 10 fold. Again, this affected the diffusion within the dilution tree. We then decided to adjust the channel width of the dilution tree to 50 μm . We predicted that the smaller channels would allow for better diffusion and mixing while flowing at a much slower rate ensuring diffusion into the cell culture chamber. Unfortunately, this has yet to be verified.

Additionally, we also noticed that during the fluorescence experiments, bubbles would form within the channels and chambers. This occurred no matter how fast or slow

the flow rate was. Most likely this is due to the channels dehydrating. We tried keeping the device humidified by submerging it in water but bubbles still occurred. For our next device iteration, we will incorporate a humidifying channel underneath the dilutions of dilutions device.

1.5.5 *Fluidic resistance analysis*

To develop each dilution of dilution iteration, we calculated the fluidic resistance of each channel from the end of the dilution tree to the beginning of the cell culture chamber and from the end of the cell culture chamber to the outlet. The fluidic resistance was calculated using equation 1.1. By calculating the resistance, we were able to design the channels so that the resistances were equal. In theory, by doing this should allow the flow within all the channels to be equal permitting sufficient mixing and diffusion of FITC-dextran and water.

1.5.6 *Comsol simulation of dilutions of dilutions device*

Due to the complications with the fluorescent studies, we decided to simulate the dilutions of dilutions device. We first simulated the device from Figure 1.5a, shown in Figure 1.9. We were able to confirm that with a flow rate of 10 $\mu\text{L}/\text{min}$, a gradient across the dilution tree and a gradient within each chamber formed. This simulation verified that a gradient formation was possible. However, due to the complexity of the design and the difficulties with the fluorescent experiments, we decided to simulate the flow of the 4 chamber dilutions of dilutions device in Figure 1.5b as well. We were able simulate a gradient within each cell culture chamber as shown in Figure 1.10b, chambers 1-4 (left-right). Although the simulations show gradient formation, we suspect that the complications with the fluorescent experiments may be due to the bubbles forming within the dilutions of dilutions device. Another possibility may be due to the length of time for

the experiment. It could be possible that for diffusion to occur via the microjets and into the cell culture chamber the gradient formation takes longer than 4 hours.

1.6 Future directions

Since we have yet to show the functionality of the dilutions of dilutions device, the next step is to incorporate a hydration channel to remove the possibility of bubbles forming within the channels. More calculations on the fluidic resistance of the channels need to be performed. The calculations should also include the channels within the tree. In addition, FITC-dextran with different molecular weights should also be tested for both experimental and simulation experiments to determine which soluble and insoluble factors play a better role in diffusion in the dilution tree and cell culture chamber.

Once gradient formation is confirmed within the cell culture chambers with multiple linear gradients, fibroblasts and hepatocytes will need to be seeded into each chamber without the gradient formation. If the cells are able to grow and proliferate within the chamber, the next step will be to apply media with different concentrations of insulin and glucagon. We would need to monitor cell damage and death from the static gradient. Glucose metabolism, albumin, urea, and P450 release from the hepatocytes will be monitored to determine how different concentrations of liver function.

Upon verifying cell growth and liver function, gas channels will be incorporated into the dilutions of dilutions device to deliver O_2 to the hepatocytes. There will be three separate gas channels that will run underneath each cell culture chamber, applying different O_2 regions to the cells. O_2 concentrations will need to be evaluated within each chamber and region with a FOXY sensor, a ruthenium based fluorescent oxygen sensor. With this addition, the interaction between O_2 and hormone gradients on liver function will be assessed.

1.6 Conclusions

A multi-gradient microfluidic device was described. We were able to demonstrate gradient formation via diffusion-based and flow-based microfluidic devices. We then combined the two techniques to create a multi-gradient diffusion-based device, called dilutions of dilutions. Through Comsol simulations, we were able to show gradient formation within the cell culture chambers of the dilutions of dilutions device. However, due to the complexity of the design, experimental gradient formation within the cell culture chamber did not occur. By thoroughly examining the fluidic resistance of all the channels that compose the device, we believe static gradient formation within the cell culture chamber is eventually possible.

1.7 References

- Abhyankar, V.V., Lokuta, M.A., Huttenlocher, A., Beebe, D.J.: Characterization of a membrane-based gradient generator for use in cell-signaling studies. Lab on a Chip. 6:389-393, 2006.
- Boyden, S.: The chemotactic effect of mixtures of antibody and antigen on polymorphonuclear leucocytes. Journal of Experimental Medicine. 115:453-466, 1962.
- Chen, H., He, Z., Bagri, A., Tessier-Lavigne, M.: The chemotactic effect of mixtures of antibody and antigen on polymorphonuclear leucocytes. Neuron. 21:1283-1290, 1998.
- Cooksey, G.A., Sip, C.G., Folch, A.: A multi-purpose microfluidic perfusion system with combinatorial choice of inputs, mixtures, gradient patterns, and flow rates. Lab on a Chip. 7:417-426, 2009.
- Dertinger, S.K.W., Xingyu, J., Li, Z., Murthy, V.N., Whitesides, G.M.: Gradients of substrate-bound laminin orient axonal specifications of neurons. PNAS. 99:12542-12547, 2002.
- Fisher, A.B., Chen, S., Barakat, A.I., Nerem, R.M.: Endothelial cellular response to altered shear stress. Am. J. Physiol. Lung Cell Mol. Physiol. 281: L529-L533, 2001.
- Foxman, E.F., Campbell, J.J., Butcher, E.C.: Multistep navigation and the combinatorial control of leukocyte chemotaxis. Journal of Cell Biology. 139:1349-1360, 1997.

- Hatch, A. Kamholz, A.E., Hawkins, K.R., Munson, M.S., Schilling A.E., Weigl, B.H., Yager, P.: A rapid diffusion immunoassay in a T-sensor. Nature Biotechnology. 19:461-465, 2001.
- Jeon, N.L., Baskaran, H., Dertinger, S.K.W., Whitesides, G.M., Van de Water, L., Toner, M.: Neutrophil chemotaxis in linear and complex gradients of interleukin-8 formed in a microfabricated device. Nature Biotechnology. 20:826-830, 2002.
- Jeon, N.L., Dertinger, S.K.W., Chiu, D.T., Choi, I.S., Stroock, A.D., Whitesides, G.M.: Generation of solution and surface gradients using microfluidic systems. Langmuir. 16:8211-8316, 2000.
- Katz, N., Teutsch, H.F., Jungermann, K., Sasse, D.: Heterogeneous reciprocal localization of fructose-1, 6-biphosphatase and of glucokinase in microdissected periportal and perivenous rat liver tissue. FEBS Lett. 2:272-276, 1977.
- Keenan, T.M., Hsu, C.H., Folch, A.: Microfluidic “jets” for generating steady-state gradients of soluble molecules on open surfaces. Appl. Phys. Lett. 89:114103, 2006.
- Kim, D., Lokuta, M.A., Huttenlocher, A., Beebe, D.J.: Selective and tunable gradient device for cell culture and chemotaxis study. Lab on a Chip. 9:1797-1800, 2009.
- Schilling, E.A., Kamholz, A.E., Yager, P.: Cell lysis and protein extraction in a microfluidic device with detection by a fluorogenic enzyme assay. Analytical Chemistry. 74:1798-1804, 2002.
- Shamloo, A., Ma, N., Poo, M., Sohm, L.L., Heilshorn, S.C.: Endothelial cell polarization and chemotaxis in a microfluidic device. Lab on a Chip. 8:1292-1299, 2008.
- Whitesides, G.M., Ostuni, E., Takayama, S., Jiang, X., Ingber, D.E.: Soft Lithography in Biology and Biochemistry. Annu. Rev. Biomed. Eng. 3:335–73, 2001.
- Yu, H., Meyvantsson, I., Shkel, I.A., Beebe, D.J.: Diffusion dependent cell behavior in microenvironments. Lab on a Chip. 5:1089-1095, 2005.
- Zicha, D., Dunn, G.A., Brown, F.A.: A new direct-viewing chemotaxis chamber. Journal of Cell Science. 99:769-775, 1991.
- Zigmond, S.H., Sullivan, S.J.: Sensory adaptation of leucocytes to chemotactic peptides. Journal of Cell Biology. 82:517-527, 1979.

Chapter 2: Islet perfusion with droplet generation for analysis with capillary electrophoresis

2.1 Abstract

In type 1 diabetes (T1), the insulin-secreting beta cells of pancreatic islets are destroyed in an autoimmune response. Typically, T1 is treated with insulin therapy; however, insulin levels can still be difficult to control due to the abnormalities in blood glucose production and requires lifelong therapy dependence. Islet cell transplantation circumvents this problem, permitting insulin independence in just a few months. Current methods to assess the function of islets prior to transplantation are limited to a static glucose incubation followed by enzyme linked immunosorbent assay (ELISA) quantification of secreted insulin. Unfortunately, these methods are time consuming and provide little information about islet function as dying islets also release insulin and the static assay does not convey any time information. Previously, our group developed a microfluidic device to allow simultaneous imaging and perfusate collection of islets. In this new work, we present a further development of incorporating on chip analysis of insulin levels via capillary electrophoresis (CE). During perfusion of stimulatory glucose, islets are characterized by fluorescence imaging of the intracellular calcium response. Within the device, the perfusate flows from the perfusion chamber to a T-channel, generating a droplet composed of fluorescein isothiocyanate-labeled insulin (FITC-insulin) and anti-insulin antibodies (Ab), using perfluorodecalin as the immiscible fluid. With an oil flow rate of 5 $\mu\text{L}/\text{min}$ and a perfusion flow rate of 2.5 $\mu\text{L}/\text{min}$, the generated droplet volume is 20-40 nL at a frequency of a ~ 8 Hz. However, due to the CE chip's limited droplet injection rate, our perfusion droplet device had to be reconfigured to allow for collection fraction. From the collection fraction, droplets can be created and injected into the CE chip.

2.2 Introduction

Diabetes mellitus (DM) is a group of metabolic disease where the body is unable to regulate glucose levels resulting in increased levels of blood sugar. There are two types of DM: type 1 (T1) and type 2 (T2). In T1, the insulin-secreting beta cells of pancreatic islets are destroyed in an autoimmune response, leading to insulin deficiency (Okubo 2008). In T2, insulin is produced but fat, muscle, and liver are resistant, eventually destroying the tissues within the body. Typically, T1D is treated with insulin therapy; however, insulin levels can still be difficult to control due to the abnormalities in blood glucose production and requires lifelong therapy dependence (Keymeulen 2005, Lin 1999). To circumvent this problem, pancreatic transplantation can stop the progression of T1 complications, however, the transplantation has a high mortality rate (Gruessner 2002).

Most recently, researchers have reported success with pancreatic islet transplantations in T1 patients, leading to independency from insulin therapy in just a few months (Shapiro 2000, Robertson 2004, Inoue 2000). Donated islets are collected from a cadaver's pancreas. The pancreas is digested with collagenase, an enzyme that breaks peptide bonds in collagen, and furthered purified to isolate the islets, Figure 2.1. After culturing, the islets are transplanted into a recipient via the portal vein in the liver, Figure 2.1. Once the islets settle in the vein, the cells are able to release insulin into the body helping to regulate the blood sugar levels.

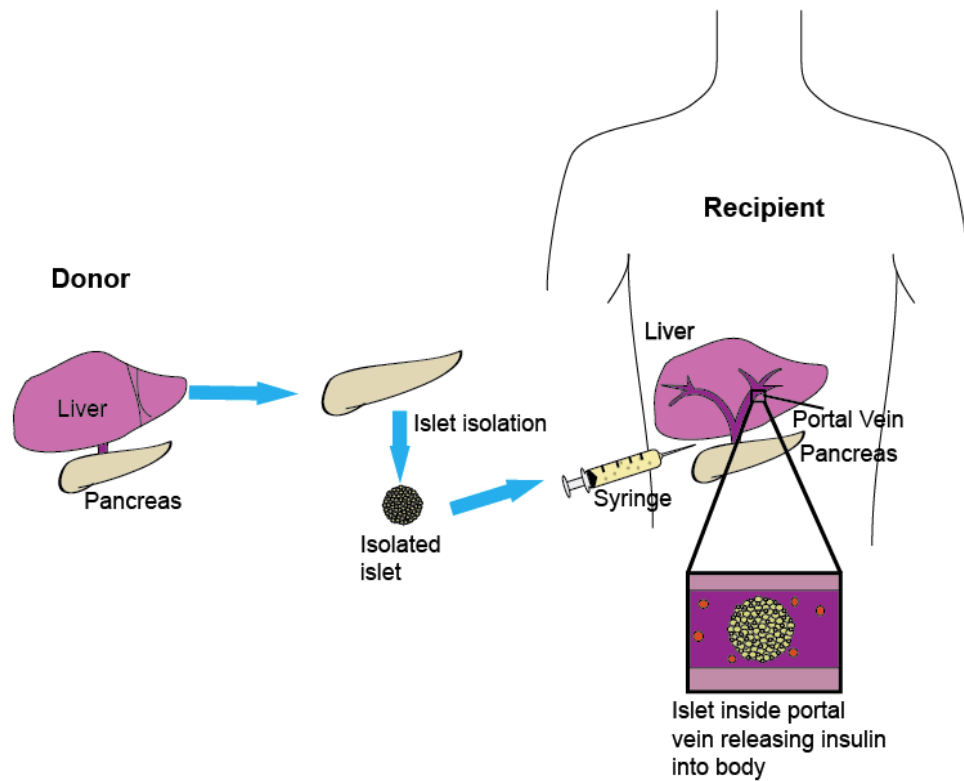


Figure 2.1. Drawing of the islet transplantation process.

Pancreatic islets are composed of a cluster of cells: beta, alpha, delta, pancreatic polypeptide (PP), and epsilon. Beta cells compose 60-80% of the cluster. As previously stated, these cells secrete insulin, a hormone that causes the body to uptake glucose from the blood for metabolic conversion and regulating long-term food intake. In addition, beta cells release amylin to help regulate glucose metabolism and short-term food intake. Alpha cells secrete glucagon, which increases blood sugar levels by converting glycogen to glucose. Delta and PP cells secrete somatostatin and pancreatic polypeptide, respectively, which help to regulate the release of insulin and glucagon. Epsilon cells secrete ghrelin, which stimulates hunger. Of the cells that compose the islets, the beta cells are the most essential in regulating insulin secretion.

When insulin is released from the beta cells, it occurs in two phases. The first phase is a rapid release of insulin to the increased glucose levels. The second phase is a gradual, slow release of newly formed insulin vesicles triggered independently of sugar (Hedeskov 1980). Figure 2.2 depicts what occurs during the 2nd phase of insulin release. Glucose enters the beta cell through glucose transporter, GLUT2. Glucose undergoes glycolysis and Krebs cycle, where ATP molecules are produced via oxidation, increasing the ATP:ADP ratio within the cell. This increase closes the ATP-sensitive potassium (K^+) channels, preventing K^+ ions from exiting the cell, creating a higher concentration of K^+ within the cell. This causes the inside of the cell to be more positive, causing the cell membrane to depolarize. Depolarization causes the calcium (Ca^{2+}) voltage channel to open, increasing the amount of Ca^{2+} to increase within the cell. An increase of intracellular Ca^{2+} ions causes the release of insulin from secretory vesicles.

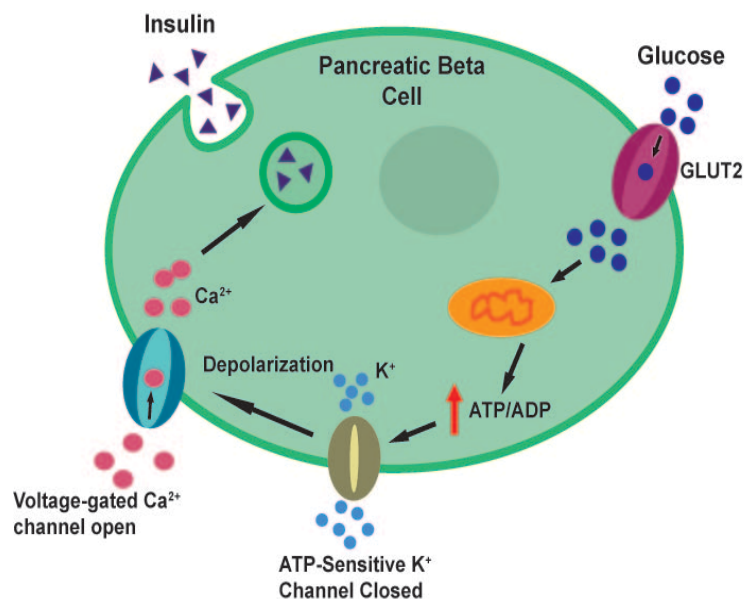


Figure 2.2. Schematic of the 2nd phase of insulin release.

By collecting the insulin release from the beta cells, we can assess the viability of the islets prior to transplantation. Current methods are limited to a static glucose incubation followed by enzyme linked immunosorbent assay (ELISA) quantification of secreted insulin (Inoue 2000). Unfortunately, these methods are time consuming and provide little information about islet function as dying islets also release insulin and the static assay do not convey any time information. Previously, our group developed a microfluidic device to allow simultaneous imaging of islet functionality and perfusate collection of islets, which monitors Ca^{2+} levels within the islets and allows insulin levels to be detected by ELISA, respectively (Mohammed 2009). Previous studies have shown that cell surface defects help to determine the functionality and viability of the cells for transplant (Maechler 2006).

To detect Ca^{2+} levels within islets, the islets are incubated in Fura-2 acetoxymethyl ester (Fura-2AM). When intracellular Ca^{2+} increases within the cell during glucose detection, Fura-2AM binds to the Ca^{2+} ions. As the Fura-2AM intensity increases, this signifies there is an increase level of Ca^{2+} ions. The increased Ca^{2+} levels indicate that insulin is being released. If there is no change in Fura-2AM intensity, then the islets are not releasing insulin, thereby they are not functioning properly. In this new work, we present a further development of this technique by combining it with an assay system that detects insulin levels via capillary electrophoresis (CE).

CE is an electrokinetic separation method that occurs in a micro- and nanofluidic channel. Figure 2.3 shows a simple schematic of a CE system. Two vials are filled with a buffer solution; one is placed with an anode electrode (source) and the other is placed with a cathode (destination). Through capillary action, the sample is introduced into the capillary. The capillary is placed back into the source vial and the analytes from

the sample migrate from the source to the destination vial by an electric field applied by the high voltage power supply. All ions are pulled through the capillary in the same direction by electroosmotic flow (Xu 1996). The separated analytes are detected by a photomultiplier tube (PMT). The detected signals are sent to a computer that then displays the data as an electropherogram. This technique can be applied to detect insulin levels from the collected perfusate samples of the islets being examined (Schultz 1995, Tao 1998).

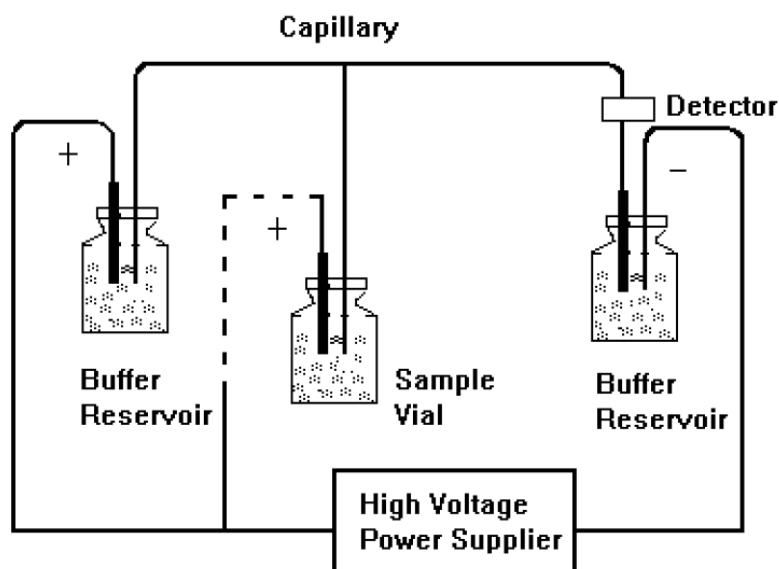


Figure 2.3. Schematic of a CE system. (From Xu 1996)

In our process to detect insulin levels from islet perfusate, a microfluidic droplet generator was designed. A droplet generator creates specific volumes of an aqueous fluid in an immiscible (oil) fluid, which can then be easily mixed, transported and analyzed (Fair 2007). There are two main types of droplet generators: flow-focusing or T-junction. In flow-focusing droplet generators, the aqueous and immiscible phases are forced through a narrow area within the device forming a droplet (Tan 2006). In T-junction

droplet generators, the aqueous channel perpendicularly intersects the immiscible phase; and as aqueous fluid flows through the junction into the immiscible fluid, the oil causes the aqueous to break into the oil stream (Thorsen 2001). In addition, T-junction droplet generators allow for easy mixing of multiple reagents (Song 2003). With both types of droplet generators, droplet size is dependent upon the flow rates of the aqueous and immiscible phases, the size of the channels, and the viscosity of the immiscible fluid (Tice 2003, Garstecki 2005, and Abate 2012).

For our process, due to the multiple reagents needed for CE analysis a T-junction droplet generator was developed. In this research, a perfusion chamber, similar to Mohammed *et al.*, was designed to connect the outlet to a T-junction droplet generator, similar to Song *et al.* The perfusate flows from the perfusion chamber to a T-channel, generating a droplet composed of fluorescein isothiocyanate-labeled insulin (FITC-insulin) and anti-insulin antibodies (Ab), using perfluorodecalin oil as the immiscible fluid. The droplet then travels to the CE chip where a PMT will detect the insulin levels. When the droplets are injected into the CE chip, bound (B) and free (F) FITC-insulin are detected and separated (Roper 2003). The ratio of bound to free FITC-insulin (B/F) quantifies the insulin levels in the perfusate. The lower the ratio is, the higher the insulin concentration. The development of an islet perfusion droplet device permits rapid determination of islet cell viability prior to transplantation, which will increase the success rate of islet transplantation.

2.3 Methods and materials

2.3.1 *Design of perfusion chamber*

An islet chamber device was developed to perfuse islet cells with constant, uninterrupted flow of basal and stimulatory glucose. This design is a smaller version of

an islet perfusion chamber previously published by our group (Mohammed 2009). As shown in Figure 2.4, the islet chamber is a multi-layer PDMS device. The bottom layer consists of an array of 500 μm diameter x 150 μm wells. Each well is separated from the next well by 60 μm . The second layer of PDMS is 1 mm thick with a 2.5 mm diameter well. The well can successfully immobilize up to 20 islets at a flow rate of 2.5 $\mu\text{L}/\text{min}$. The top layer contains a rectangular channel 11 mm x 550 μm x 250 μm that introduces the perfusate to the chamber at one end and collects at the other end of the channel. The top layer also has a port in the middle of the rectangular channel, directly above the chamber, to allow for easy delivery of islet cells to the device.

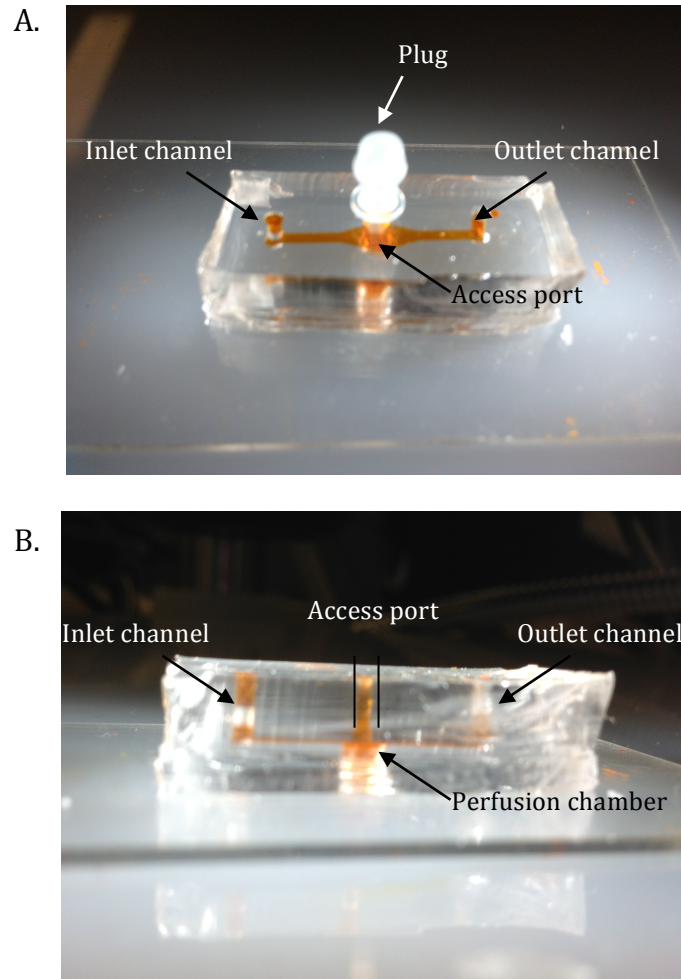


Figure 2.4. Images of 5 μ L perfusion chamber. A) Top view of the perfusion chamber showing the placement of the plug to the access port. B) Cross section view of perfusion showing the 3 layer of the device.

2.3.2 *Fabrication of perfusion chamber*

The perfusion chamber is fabricated off of two different masters using standard photolithography methods. Each master was made with a different photomask and SU-8 protocol. For the first layer, SU-8 2150 was spun at 500 rpm for 10 s and then at 3000 rpm for 30 s onto a 3" silicon wafer. The wafer underwent a prebake of 65° C for 5 minutes and 95° C for 30 minutes, and then exposed to UV light at 260 mJ/cm². After exposure, the wafer was baked at 65° C for 5 minutes and 95° C for 12 minutes and then

fully developed to expose the design. The top layer was fabricated by spinning SU-8 2150 at 500 rpm for 10 s and then at 2000 rpm for 30 s onto a 3” silicone wafer. The wafer was baked at 65° C for 7 minutes and 95° C for 60 minutes and exposed to UV light at 370 mJ/cm². Upon exposure, the silicon wafer was baked at 65° C for 5 minutes and 95° C for 20 minutes. The wafer was developed for 20 minutes with SU-8 developer (Microchem).

After development of both wafers, PDMS was premixed at a ratio of 10:1 polymer base and curing agent, poured onto each master, and cured at 85° C for 1.5 hours. If needed, the PDMS was degassed again prior to curing. For the middle layer, a compression molding method was used. A clean 3” silicon wafer was placed onto a balanced hotplate covered with aluminum foil. Four 25 mm x 75 mm x 1 mm glass slides were placed onto the silicon wafer and taped to the aluminum foil. Premixed PDMS was poured onto the silicon wafer and bubbles were removed with a rubber blower (Ted Pella, Inc.). A transparency film (3M) was placed on top of the silicon wafer followed by a glass dish and weight. The dish was placed on top of the taped glass slides and the whole thing was baked at 75° C for 1.5 hours. Upon curing, the PDMS was removed, giving the desired height of 1 mm for the large perfusion well. A 2.5 mm hole punch was used for the well. For the top layer, PDMS was premixed at a ratio of 10:1 polymer base and curing agent, poured onto each master, and cured at 85° C for 1.5 hours. Once cured, the PDMS mold was removed and a 14 gauge was punched into the inlet.

For bonding, the middle and top layer were cleaned and prepared with tape. Each side of the PDMS was plasma treated and put into contact with each, Figure 2.1. This section was then placed onto a ceramic hotplate at 120° C for 30 minutes. Once cooled to room temperature, the islet port was punched into the middle of the large well, Figure

2.1b. The two layer PDMS and bottom layer, were cleaned with tape, plasma treated, and baked at 120° C for 30 minutes.

2.3.3. Computer simulation of perfusion chamber

Using Comsol software (Comsol, Inc), the flow within the perfusion chamber was simulated. Initially, a perfusion chamber with a diameter of 3.6 mm was used for perfusing islet cells. After several experiments it was quickly determined that a simulation of the chamber needed to be performed due to the irregularity of the islets Ca^{2+} response.

To perform the simulation of fluid flow within the chamber, a 3D design of the chamber from AutoCAD was imported into the software and the laminar flow tool was selected. The 3D module was selected. The flow was set to incompressible flow and the inlet and outlet were selected. Inlet channel was set to normal inflow velocity at 2.5 $\mu\text{L}/\text{min}$ and the outlet flow was set to pressure at 101325 Pa, or atmospheric pressure. Once the simulation was generated, a slice of the velocity results in the yz-plane was obtained. Streamlines of the fluid flow were generated to visualize the fluid direction.

2.3.4 Krebs Ringer Buffer

Krebs Ringer Buffer (KRB) was used for all experiments performed with the perfusion chamber and droplet generator. To validate the droplet generation KRB was used in place of FITC-insulin and Ab. In a 1 L flask, the following chemicals were added: 5.96 g of HEPES (Sigma), 6.72 g of NaCl (Sigma), 2.02 g of NaCHO_3 (Sigma), 0.3728 g of KCl (Sigma), 0.2033 g of $\text{MgCl}_2 \cdot 6\text{H}_2\text{O}$ (Fisher), and 1.0 g of BSA (Sigma). Distilled was added to the flask until it was filled to 1 L. Afterwards, 0.3675 g of $\text{CaCl}_2 \cdot 2\text{H}_2\text{O}$ was added and the solution was stirred. The pH level was monitored and adjusted to 7.3-7.5. 2 mM of glucose (Sigma) was added to the flask. This is the basal solution (KRB2) used

for all experiments. For the stimulant KRB, 14 mM of glucose was added to a 50 mL conical tube of the 2 mM KRB (KRB14).

2.3.5 Pancreatic islets isolation and culture

Pancreatic islet cells were isolated from C57B6 mice. Mice were anesthetized with an overdose of vaporized isoflurane and sacrificed by cervical dislocation. Afterwards, they were laid on their back and their abdomen was thoroughly disinfected with 70% ethanol (EtOH). A “V” shape beginning from the pubic region to the diaphragm was cut into the mice to expose all organs in the peritoneal cavity opened the abdominal wall. The xiphoid was removed and gauze was used to secure the liver in place, exposing the common bile duct. The mice were then placed under a dissecting microscope and the bile duct was clamped with a hemostat near the duodenum. A 5 ml syringe of 0.375 mg/ml colleenase P (Sigma), with a 30 gauge needle, was injected through the bile duct allowing 2-3 ml of colleenase into the pancreas. After the pancreas is distended, it is removed and placed directly into a 50 ml conical tube of 5 ml of the enzyme solution and placed on ice. 3-6 pancreases could be placed into a conical tube, the pancreas from the remaining mice were removed in a similar manner. Once the desired number of pancreases was collected, the conical tube was placed into a 37° C water bath for 11 minutes. The conical tube was then filled halfway with 4° C HBSS (Cellgro), vigorously shaken for several seconds to further digest the pancreases. The conical tube was then placed into a centrifuge and spun at 1000 rpm for 1 minute. The contents in the conical tube were washed 3 more times with HBSS and centrifuged. Next, the pellet in the conical tube was separated in a ficol gradient (1.108, 1.096, 1.069, 1.037) (Cellgro). The tube was placed into a centrifuge and spun at 1800 rpm for 15 minutes at 4° C. Afterwards, islets were collected between 1.096 and 1.069 and washed two times in

RPMI 1640 (Gibco) with 10% fetal bovine serum (Invitrogen) and 1% penicillin/streptomycin (Invitrogen). Islets were cultured in 100 mm petridishes with RPMI medium at 37° C, 5% CO₂. Islets kept in petridishes could be used for up to 4 days after isolation with daily media change. Typically, one mouse pancreas could yield 100-300 islets. Protocols for animal experiments were approved by University of Illinois at Chicago Office of Animal Care and Institutional Biosafety.

2.3.6 Incubation of islet cells in Fura-2AM

The calcium (Ca²⁺) response of islets were determined by treating the cells with Fura-2 acetoxymethyl ester (Fura-2AM). For each experiment, 10 µL of Fura-2AM were put into a small petri dish of 2 mL KRB2. 20 islets were selected and incubated in the petri dish at 37° C for 30 minutes.

2.3.7 Perfusion chamber experimental setup

Prior to each experiment, the perfusion chamber was conditioned with ethanol to absorb into the channel walls for 15 minutes. The chamber was then washed out to remove ethanol with KRB2. Once the islets were incubated, 10 were selected and put into the chamber via the top port. When the islets have settled to the bottom of the chamber, the port was plugged with a closed tip connector fabricated in house.

A syringe filled with KRB14 was placed onto a Chemyx Fusion 100 syringe pump and connected to tygon tubing (Cole-Parmer). At the end of the tubing, a metal connector was inserted and a 2 inch tygon tube filled with KRB2 was inserted into the connector. The KRB2 tubing was inserted into the inlet of the perfusion chamber. The perfusion chamber was then placed onto an inverted epifluorescenc microscope (Leica DMI 4000B) and perfused with KRB at a flow rate of 2.5 µL/min at 37° C.

The islets were observed with a 20x objective. Dual wavelength Fura-2AM was excited at 340 and 380 nm, with the changes of Ca^{2+} were expressed as a ratio. The excitation wavelengths were controlled by excitation filters mounted in Lambda DG-4 wavelength switcher. Emission of Fura-2AM was filtered with a Fura2/FITC polychroic beamsplitter and double band emission filter. SimplePCI software was used for image acquisition and analysis.

2.3.8 Design of droplet generator device

A droplet generator device was developed to combine three reagents, or aqueous phase: islet cell perfusate, fluorescein isothiocyanate-labeled insulin (FITC-insulin) (Sigma), and anti-insulin antibodies (Ab) (Meridian Life Sciences). Droplets of the three reagents were formed via a T-junction channel with 10:1 (v/v) ratio of perfluorodecalin, mixture of *cis* and *trans*, 95% (Sigma) and perfluorooctanol (Sigma) (PFD) as the immiscible phase. The device contains a perfusion chamber, as described above, and three other inlet channels that join to make a T-junction droplet generator, Figure 2.5. The channels of the three aqueous phases have a width of 75 μm with a junction point, where the channels meet, of 75 μm . The immiscible phase has a width of 150 μm . The entire droplet generator has a height of 100 μm . The dimensions of the device were designed to generate droplets of about 20 - 40 μL in volume.

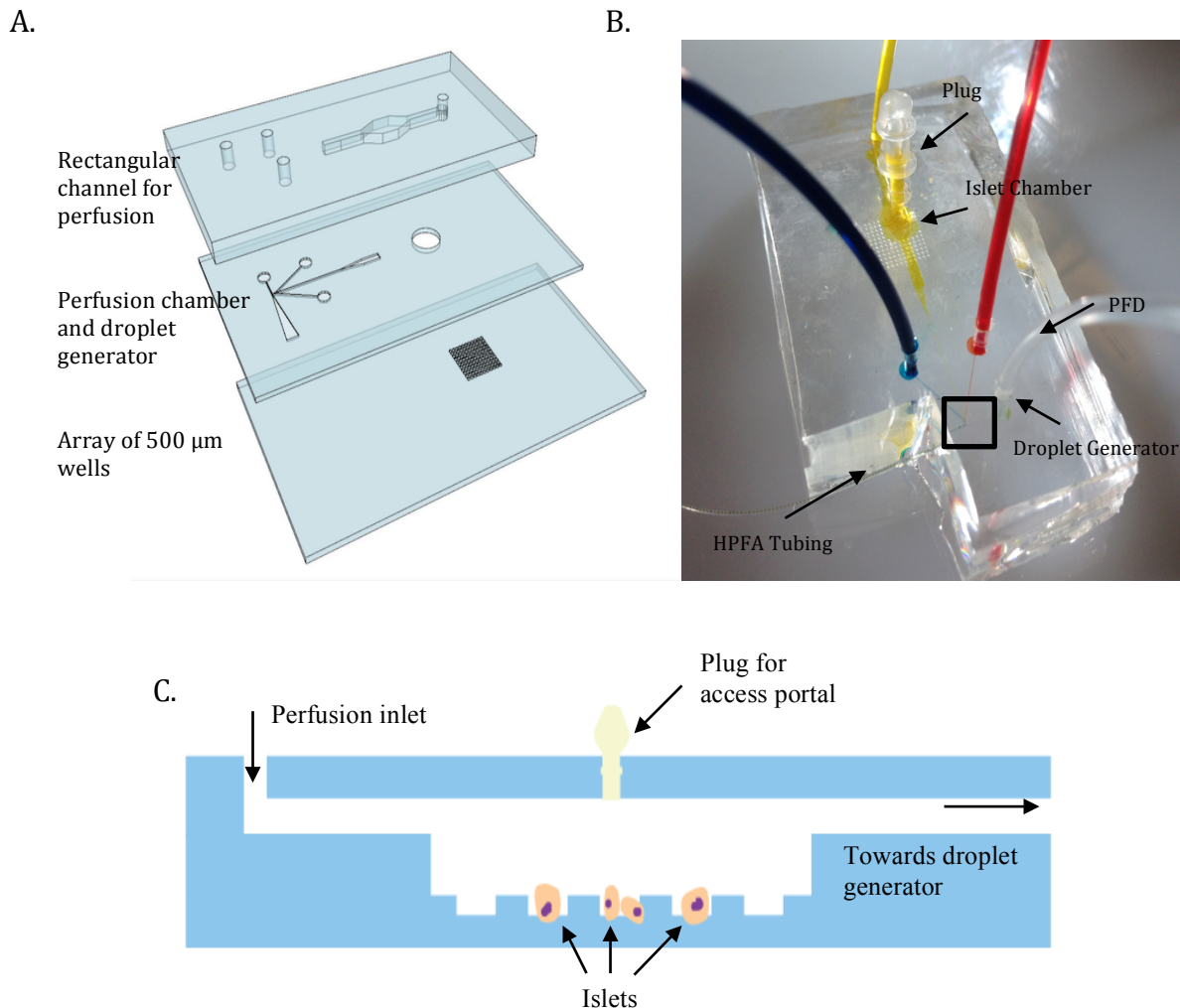


Figure 2.5. Droplet generator device. A) A sketch of the 3 layers of the droplet generator device. B) PDMS droplet device with food dye to visualize the channels. C) Cross-sectional sketch of perfusion chamber.

2.3.9 Fabrication of droplet generator

To fabricate the droplet generator device, three masters were used. Standard photolithography methods were used for each master. The first master, the bottom layer of the device, contained an array of wells for islet trapping. Fabrication method was previous described in section 2.3.2. The second master, the middle layer, has the droplet generator and a 2.5 mm perfusion well. For the master, SU-8 2100 was spun at 500 rpm for 10 s and 3000 rpm for 30 s unto a silicon wafer. The wafer was baked at 65° C for 5 minutes and 95° C for 20 minutes. After baking, a photomask was placed over the silicon wafer and exposed to energy of 240 mJ/cm². After exposure, the silicon wafer was baked

at 65° C for 5 minutes and 95° C for 10 minutes. The master was developed to remove the unexposed features for 10 minutes. The third master, the top PDMS layer, had the same dimensions as the rectangular channel of the perfusion chamber and fabricated using the same methods as described above.

Upon development of the three layers, PDMS was poured and cured unto the bottom and top masters. The mold for the middle layer was fabricated using compression molding. This master was placed unto a hotplate. Four glass slides, 75 x 25 x 1mm, were placed and taped into place around the droplet generator design. PDMS was poured unto the master and a transparency film (3M) was placed on top of the master and slide combination. A glass block was placed on top of the transparency allowing the edges of the block to be aligned on top of the slides. The compression molding allowed the PDMS, the 2.5 mm well thickness, to be 1 mm thick, equating to a volume of 5 μ L. Once all PDMS layers were cured, the top and middle layer inlets were punched with a 14 gauge punch and bonded together via corona treatment of both sides that were put into contact. After bonding, the two PDMS layers were placed unto a ceramic hot plate at 120° C for 20 minutes. This ensured that the layers were tightly bonded. Once the layers cooled, a 12 gauge was used to punch a hole via the 2.5 μ m well through the center of the rectangular channel. These two layers were then bonded to the bottom layer using the corona treater and baked at 120° C for 20 minutes.

After the device cooled to room temperature, Novec 1720 (3M) was perfused into the device until all visible bubbles were gone and channel walls were entirely wet. Once all bubbles were gone from the device, the device was placed unto a hot plate at 130° C for 15 minutes.

Once cooled, PDMS was mixed and baked at 65° C until the PDMS became tacky. The fanned out channel of the droplet generator, Figure 2B, was then cut out to expose the side of the droplet generator outlet. A 150 OD μm x 360 OD μm high purity perfluoroalkoxy alkane tubing, HPFA (Upchurch Scientific) was inserted into the outlet and “glued” into place using the tacky PDMS. The device was then baked at 65° C for 30 minutes.

2.3.10 *Experimental setup of droplet generator*

Prior to experiments, the droplet generator was infused with KRB2 for 15 minutes. Islet cells were incubated in Fura-2AM, as previously described. The device was rinsed with KRB2 once more and islets were placed into the perfusion chamber through the port. Once cells settled to the bottom, a plug was put into the port. 3 syringe pumps (Chemyx) were used to perfuse into the inlets. For the perfusion chamber, a syringe was prepared as previously described in section 2.3.7 but with a 4 inch tube of KRB2. This syringe was placed into its own pump. The flow rate of this syringe was set at 2.5 $\mu\text{L}/\text{min}$. For the FITC-insulin and Ab channels (Ch1 and Ch2), KRB2 was used as a substitute for the reagents; syringes were prepared, and placed into a separate syringe pump. The flow rate for this syringe pump was set at 1 $\mu\text{L}/\text{min}$. Another syringe pump was used for the immiscible phase and set at a flow rate of 5 $\mu\text{L}/\text{min}$. With all 3 syringe pumps operating, and after equilibration, droplets were generated at an estimated rate of 8 Hz with an estimated volume of 20 μL .

After droplet generation was confirmed via the microscope eyepiece, the fluorescent detection, acquisition, and analysis of Fura-2AM of the islets was collected. This process was previously described in section 2.3.7.

2.3.11 *Size and frequency of droplets*

In order to determine the size of the droplets, an image was taken of a single droplet. Using ImageJ, a line was drawn across the surface area of the channel to determine the number of pixels across the channel. The ratio of actual channel length to the number of pixels (actual channel length/number of pixels) was used to determine the size of the droplet based off the number of pixels in the length and width of droplet.

Droplet frequency was determined by taking a movie of the droplets as they were generated at a known frames per second (fps). The number of frames per droplet was determined and divided by the fps of the movie.

2.3.12 *Capillary electrophoresis chip*

For analysis of the droplets generated from the islet generator device, a glass capillary electrophoresis (CE) chip was used. Our collaborators at University of Michigan, Ann Arbor, fabricated the CE chip.

To fabricate the chip, standard glass etching methods were used. A photomask was aligned atop a glass chip coated with chrome and positive photoresist and UV exposed. The chip is then dipped into developer to remove the photoresist in the exposed area and then dipped into chrome etching solution to remove chrome from the exposed area. Etching solution is composed of double distilled water (ddH₂O), nitric acid (HNO₃), and 49% hydrofluoric acid (HF). The channel depth is dependent on the etching rate. To obtain a depth of 15 μm at an etching rate of 0.6 μm/minute, etching time would be 25 minutes. After the chip has been etched, the chip is cleaned with ddH₂O and holes with a diameter of 360 μm are drilled into the chip. The chips are cleaned with acetone and ddH₂O to remove remaining photoresist and particles; followed by a dip in etching solution to remove remaining chrome coating. The chip and a blank glass plate are cleaned with soap water, treated with Piranha solution 3:1 (v/v, sulfuric acid/hydrogen

peroxide) for 20 minutes, and then treated with RCA solution 5:1:1 (v/v/v, water/ammonium hydroxide/hydrogen peroxide) for 40 minutes. After the chip and plate are rinsed with deionized water, the two are put into conformal contact in between two ceramic plates, placed inside a Neytech Centurion Qex furnace, and baked at 640° C for 8 hours. Epoxy rings and plastic microfluidic reservoirs (Upchurch Scientific) are aligned over the glass chip holes and baked at 175° C for 1 hour so that the reservoirs are bonded to the chip. Two 1 mm sections of 75 µm OD x 360 µm fused silica tubing were glued into the side of the glass chip. One tube was for extracting droplets and the other is for balancing the pressure differential within the chip. The chip is examined under a microscope to ensure the channels are free of all particulates so that the channel resistance is unaffected.

2.3.13 Preparation of balanced salt solution and immunoassay buffer

For all droplet analysis experiments, balanced salt solution (BSS) was used instead because KRB can cause HPO_4^{2-} within the CE chip. In a 1 L flask, the following chemicals were added: 7.3050 g of NaCl (Sigma), 0.4398 g of KCl (Sigma), 0.2440 g of $\text{MgCl}_2 \cdot 6\text{H}_2\text{O}$ (Fisher), 0.3528 g of $\text{CaCl}_2 \cdot 2\text{H}_2\text{O}$ (Sigma), 4.4800 g of tricine (Fisher), and 0.700g of BSA (bovine serum albumin) (Sigma). The flask was then filled to 1 L with Milli-Q water. This buffer was used to perfuse islets with basal and stimulant solution.

For the immunoassay buffer (IB), the following chemicals were added to a 500 ml flask: 1.7532 g of NaCl (Sigma), 0.1861 g of EDTA (Fisher), 1.7920 g of tricine (Fisher), 0.5000 g of tween 20 (Sigma), and 3.5 g of BSA (Sigma). The flask was filled to 500 ml. The IB was used to make the FITC-insulin and Ab solution. 1.8 µl of FITC-insulin was

added to 2 ml of the buffer and 3.8 μl of Ab was added to 2 ml of the buffer in each in their own respective tube.

2.3.14 Droplet analysis by capillary electrophoresis

In order to analyze the droplets generated by the droplet generator device, an extraction device was developed. The tubing from the droplet generator connected directly to the extraction device, which in turn is connected to the CE chip. The extraction device, made of PDMS, is designed to allow the droplets to enter the CE chip's extraction tube. Our collaborators at the University of Michigan, Ann Arbor, fabricated this device (Figure 2.6).

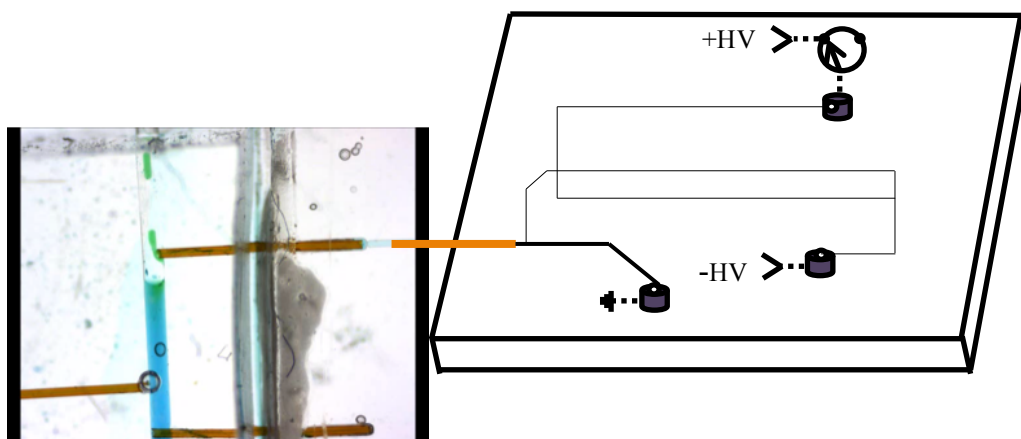


Figure 2.6. Example of the CE chip fabricated by our collaborators at the University of Michigan in Ann Arbor. Image on the left is the extraction device. Here green droplets are extracted into the CE chip, right. Right image shows a schematic of the CE chip.

The CE chip and extraction device was placed into a microscope with fluorescent optics. A 20 mW Ar^+ laser was directed onto a 500 nm long-pass mirror through an objective. The emission light was collected, passed through the long-pass mirror, and a 520 nm filter. The light was filtered with a 1 mm pinhole and detected with a PMT. Software written in Labview was used to control and collect data.

Figure 2.6 shows the voltage arrangement for the injection of the droplets. A channel connected to the extraction tube was grounded and a waste reservoir was held at negative high voltage via a high voltage power supply. During injection, the voltage gate was floated to allow the droplet to enter the detection channel. After injection, the voltage was held at ground allowing the droplets to enter the waste reservoir. As the droplets are detected by the PMT, the signal is collected to determine the B and F FITC-insulin levels. The ratio of the bound to free FITC-insulin (B/F) quantifies the amount of insulin in the perfusate.

2.3.15 Islet perfusion chamber mixer design and fabrication

After attempts to use the droplet generator device failed, we decided to develop an islet perfusion chamber with inlets for FITC-insulin and Ab that connected and mixed with the perfusate, Figure 2.7. Once the three mixed together, the reagents exited the device via microbore tubing (Cole Parmer) and collected off chip. Described below.

The device was fabricated using the same techniques as described in section 2.3.9. Fabrication consisted of the three masters: well array, perfusion chamber and reagent mixer, and rectangular perfusion channel. The same soft photolithography methods were used for each layer. The bonding process was also done in the same manner as 2.3.9.



Figure 2.7. Image of the islet perfusion chamber mixer device.

2.3.16 Droplet collection for capillary electrophoresis

The device setup for experimentation was identical to the droplet generator setup. The same flow rates were used for each inlet, omitting the use of the oil channel. Instead of 10 islets added to the perfusion chamber, 20 were used instead to increase the insulin intensity levels detected by the CE chip.

Once the 3 reagents are mixed and exiting the device, fraction collection was used. Using a PCR plate, sample was collected for 2.5 minutes. A total of 10 wells were collected. After collection, the plate was placed onto a platform, Figure 2.8. PFD was deposited on top of each sample well. The density of the oil is much lighter than the sample so it remains atop the sample if undisturbed. 150 OD μm HPFA tubing was connected to a xyz stand and syringe pump. The tubing hung from the stand and “dipped” down into the first well of the plate. The syringe pump was set at a withdraw rate of 2 nL/min and a Labview software was used to move the xyz stand. The program was

designed to dip the HPFA tube into the sample and then collect the oil atop the sample while the syringe pump withdrew. This process generated the droplets needed for the CE chip.

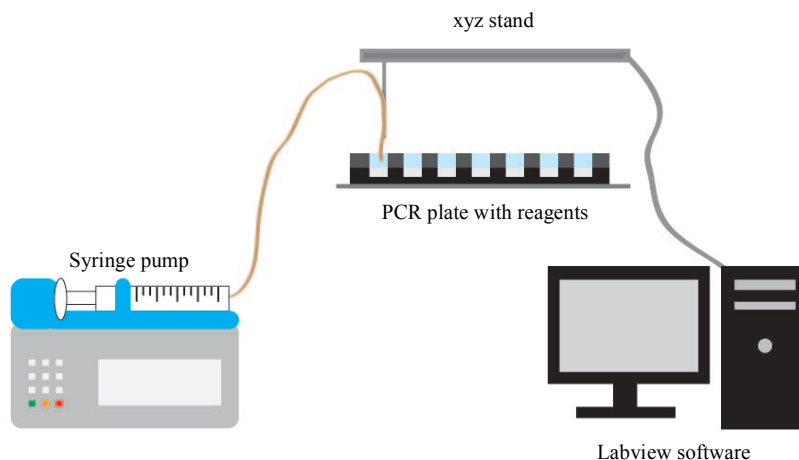


Figure 2.8. Schematic of the droplet collection from fraction collection.

After the samples were collected from each well, the tube was connected a separate syringe pump and to the extraction device. The extraction device was connected to the CE chip. The syringe pump then pumped the droplets from the tubing into the CE chip.

2.4 Results

2.4.1 *Comsol simulation of perfusion chamber*

Flow in a 20 μL and 5 μL perfusion chamber was verified using Comsol, Figure 2.9.

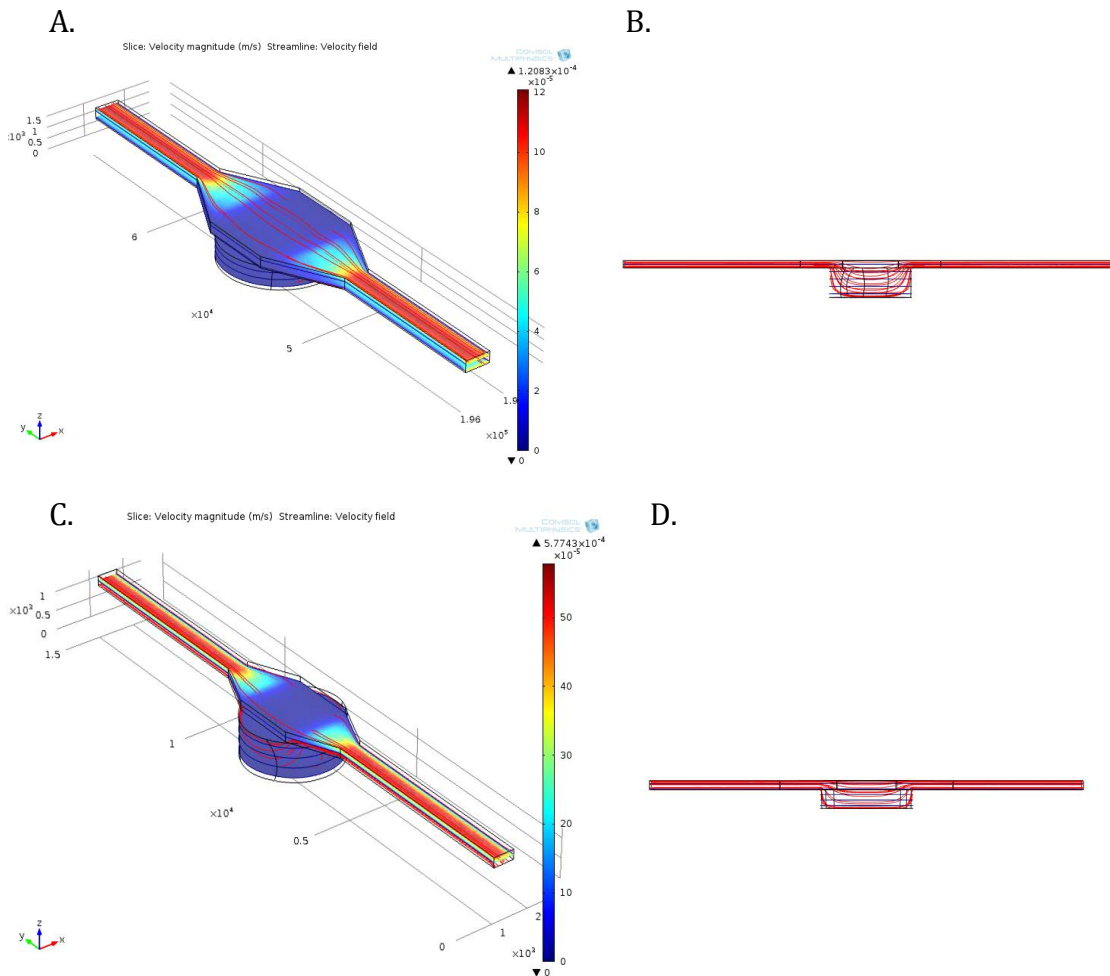


Figure 2.9. Comsol simulation of flow within the 20 μL and 5 μL perfusion chamber. The velocity flow (A) and the streamline flow of the 20 μL perfusion chamber. The velocity flow (C) and the streamline flow (D) of the 5 μL perfusion chamber.

2.4.2 Calcium response of islets with perfusion chamber

10 islets were added to the perfusion chamber through the access port. The glucose flow rate was 2.5 $\mu\text{L}/\text{min}$. Islet cells were stimulated by basal, 2 mM, glucose and then stimulatory, 14 mM, glucose. The Ca^{2+} response of the 5 μL chamber, $n=2$, is shown in Figure 2.10.

Calcium Response with 5 μL Chamber

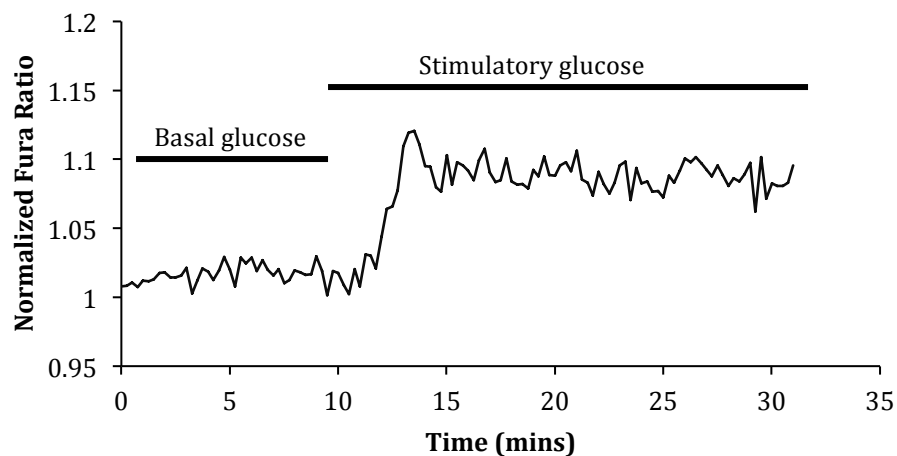
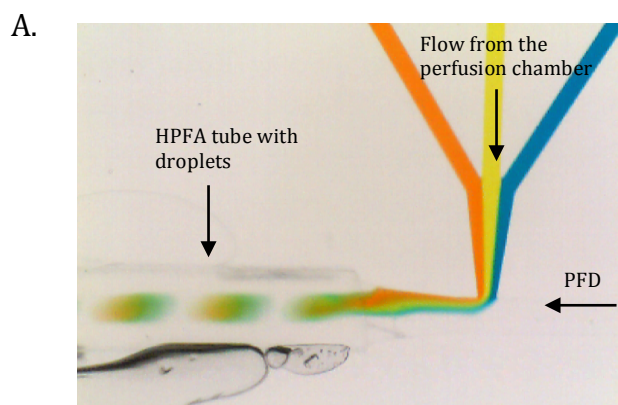


Figure 2.10. Ca^{2+} response of 5 μL perfusion chamber, $n=2$.

2.4.3 Droplet generator device

The droplet generator device with the 5 μL perfusion chamber was able to generate droplets with a volume of 20 – 40 nL and a frequency of 8 Hz, Figure 2.11. Yellow dye is fluid flow from the perfusion chamber at 2.5 $\mu\text{L}/\text{min}$. Red and blue food dyes represent FITC-insulin and Ab reagents at a flow rate of 1 $\mu\text{L}/\text{min}$. The PFD channel flowed at 5 $\mu\text{L}/\text{min}$.



B.

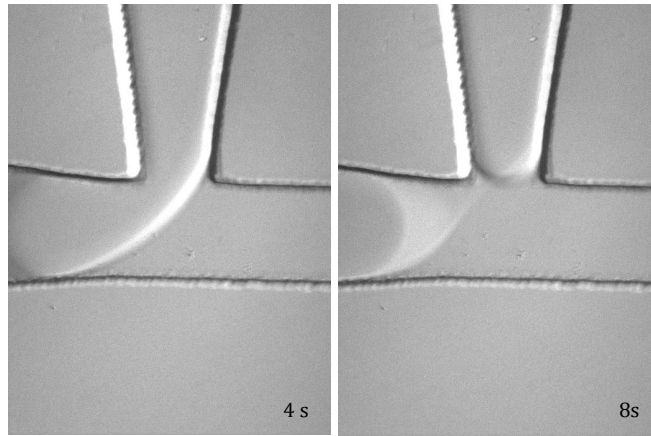


Figure 2.11. Images of the droplet generator device. A) Shows the generation of the droplets from the 3 aqueous phases and oil phase. B) Time lapse images of droplet generation at 8 Hz.

2.4.4 Calcium response with droplet generator device

The 5 μL perfusion chamber droplet device was used to verify simultaneous droplet generation and islet perfusion. Once islets were added to the chip and tubing connected to the inlets, droplet generation was confirmed via the microscope eyepiece. After confirmation, the islet fluorescent experiments began and the results obtained of $n=1$, Figure 2.12. Once a Ca^{2+} response was obtained, droplet generation as confirmed again.

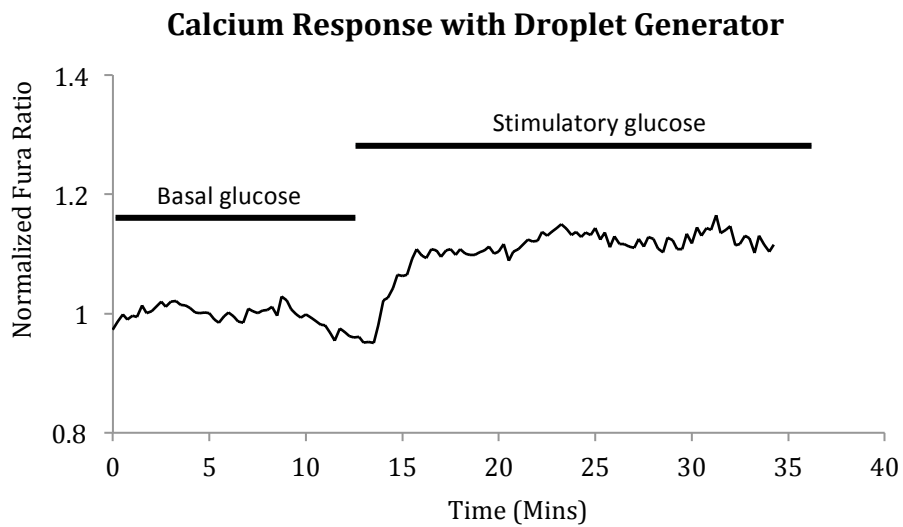


Figure 2.12. Ca^{2+} response with droplet generator device. $N=1$.

2.4.5 Electropherogram with droplet generator device and CE chip

20 islets were added to the perfusion chamber of droplet generator. After 10 minutes of equilibration and droplet confirmation, the tubing of the device was connected directly to the CE chip. The results obtained from the CE chip are shown below in Figure 2.13.

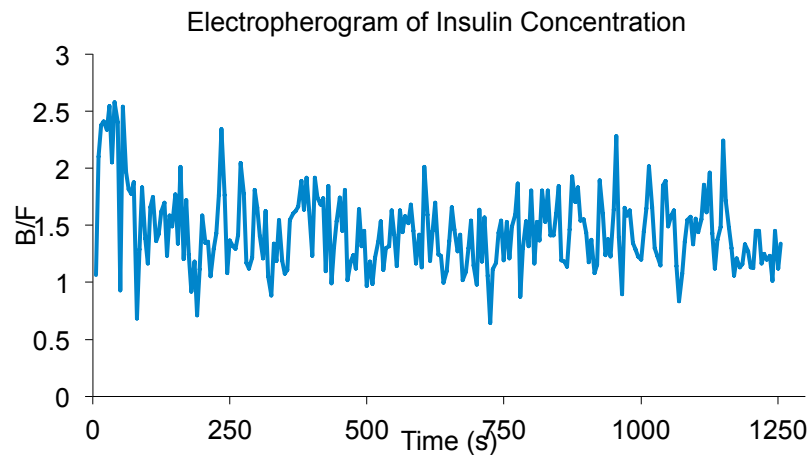


Figure 2.13. Electropherogram of insulin concentration with droplet generator connected.

2.4.6 Results with islet perfusion chamber mixer device

Islets were added to the islet perfusion chamber mixer device. Three experiments were performed and Ca^{2+} responses of the islets were recorded. The fraction was collected every 2.5 minutes for 25 minutes. The Ca^{2+} response from the three experiments is shown in Figure 2.14. The fraction was then collected into droplets and perfused into the CE chip where electropherograms were recorded (not shown).

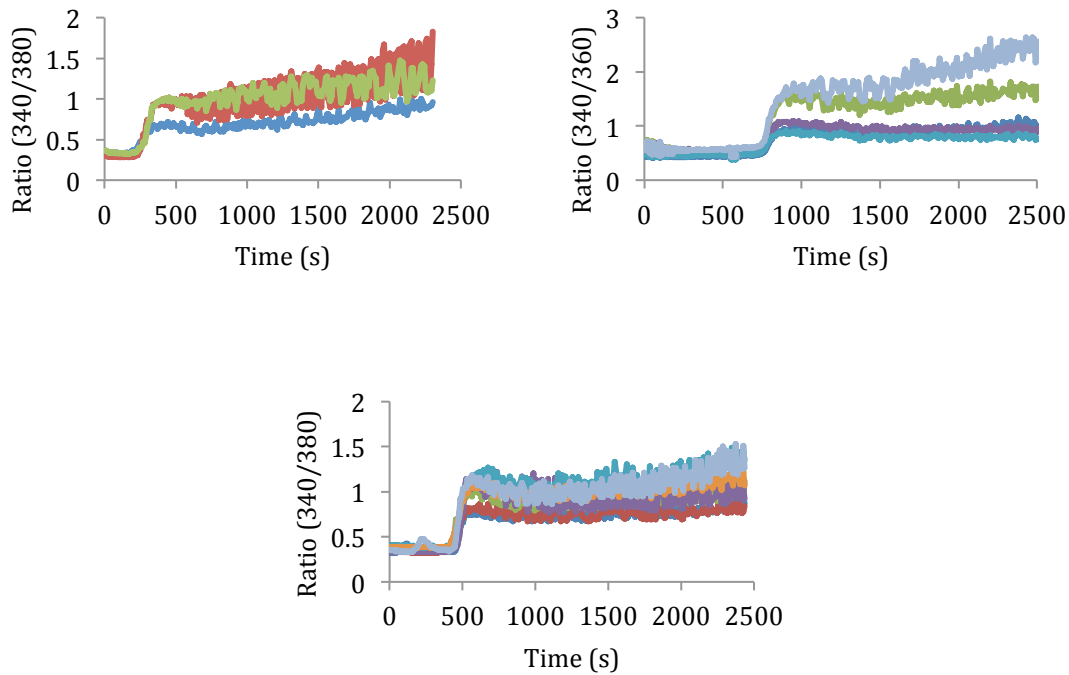


Figure 2.14. Three experiments of Ca^{2+} response in the islet perfusion mixer device.

2.5 Discussion

2.5.1 *Comsol simulation of perfusion chamber*

Initially, 5 mm OD x 1 mm H chamber (a volume of 20 μL) was used for the islet perfusion chamber, but we noticed the amount of time it took for the glucose to wash out of the chamber took much longer than expected. The longer wash time meant the longer amount of time for the islets to respond to the glucose. Comsol was used to show the fluid flow within the chamber and verify the flow was indeed uniform. Modifications were made to reduce the chamber size to a volume of 5 μL and verified with Comsol for flow uniformity to obtain the current chamber size of 2.5 mm OD x 1 mm H.

2.5.2 *Calcium response in perfusion chamber*

The Ca^{2+} response of 10 islets was evaluated in the 5 μL chamber. From Figure 2.10, we were able to observe 1st and 2nd phase of the insulin release when the glucose switched from basal to stimulant. After the 2nd phase, the insulin release maintains

constant which is clear from the steady Ca^{2+} response. This experiment was essential to verify that the 5 μL chamber was able to provide sufficient perfusion to the islets. Wash time for the perfusion chamber is 2 minutes.

2.5.3 Droplet generator device

After confirming that the 5 μL perfusion chamber was able to provide adequate perfusion flow to the islets within the chamber, a 3-inlet T-junction droplet generator was incorporated into the chamber. To generate the droplets, the droplet device went through several iterations and flow rates. The final design, shown in Figure 2.5, was chosen due to producing the most stable droplets. Initially, the flow rates were 10 fold higher than what was previously described. The flow rates decreased 10 fold due to the speed and size of the droplets produced. In fact, the droplet frequency was much too fast for our camera to adequately capture. Also, we determined that the droplet frequency was much too quick for the CE chip. We reduced the flow rates to their current rates. By doing so we were able to obtain droplets of 20 – 40 nL at a frequency of 8 Hz.

2.5.4 Calcium response with droplet generator

Islets were added to the perfusion chamber of droplet generator device. Prior to fluorescence imaging, droplet formation was confirmed. Once we were able to confirm the droplet formation, we quickly began the fluorescent imaging of the Ca^{2+} response. The Ca^{2+} response of the droplet generator device, Figure 2.12, shows that the perfusion chamber was able to switch from basal to stimulatory glucose. The 1st phase and 2nd phase were also clearly evident in the figure. After the Ca^{2+} response experiment, we continued to run the syringe pumps to verify that droplet formation was still occurring.

During several experiments, we realized that if there were any problems with the droplet generation of the device, it would quickly affect perfusion chamber. The problem

that occurred most frequently was oil back flow into the chamber. If this occurred during fluorescent imaging, the graph of the Ca^{2+} response would quickly display irregular values.

2.5.5 Droplet analysis with CE chip

With our University of Michigan collaborators, we connected the outlet tubing of the droplet generator device to the CE chip. We increased the number of islets to 20 to increase the concentration of insulin produced by the device so that the CE chip could properly detect the insulin levels. We discovered that though the CE chip was extracting the droplets, majority of the droplets were going to waster. When we ran the electrophoresis, there were able to detect peaks even though no fluorophore had been placed directly into the CE chip. This indicated that some solution definitely extracted across the detection channel. However, the B/F ratio was very unstable, as shown in Figure 2.10. This could be caused by poor/unstable mixing in the islet device, by problems with the extraction (oil possibly extracting into the electrophoresis chip), or a combination of both.

2.5.6 Islet perfusion mixer device

After realizing the CE chip was not extracting the droplets very well, we decided to collect fractions of the perfusate, Ab, and FITC-insulin solution. Since we would be collecting fractions, we did not need the droplet generator portion of the device. Instead, we incorporated a long winding channel that will allow for mixing of the perfusate, Ab, and FITC-insulin. We were able to collect fractions of the mixed reagents while simultaneously measure the Ca^{2+} response of the islets. In Figure 2.14, 3 graphs are depicted of the Ca^{2+} response from 3 different experiments done at University of Michigan.

Unfortunately, due to difficulties with the CE chip during our 2nd University of Michigan visit, we were not able to successfully extract droplets of the collection fraction into the chip. Oil was frequently detected in the detection channel of the CE chip, which created noise in the electropherogram. This can be an on going problem with CE chips. It would be best to test each CE chip before use with different standards to verify the chip will work properly. Since only 3 samples of fraction were collected, more experiments with the CE chip need to be performed.

2.6 Future directions

The next phase of this research will be to collect fractions for study with the CE chip. Once we can show that the CE chip can detect the B/F ratio of insulin, we would like to expand this research by designing a droplet generator device capable of injecting droplets directly into the CE chip. For this to occur, the droplet generator would need to generate droplets at a much slower rate. The perfusion chamber would need to be much smaller than 5 μ L. The aqueous and oil channels would need to be smaller than 75 and 150 μ m, respectively. By making these channels smaller, we should be able obtain much smaller droplets at a slower frequency. In addition, we may also want to incorporate valves into the device to reduce the number of droplets injecting into the CE chip.

2.7 Conclusion

In this research, we developed a microfluidic perfusion chamber that connected to a T-junction droplet generator capable of generating droplets of islet perfusate, FITC-insulin, and Ab. We were able to simultaneously monitor the Ca^{2+} response of islets and generate droplets. However, due to the difficulties of injecting droplets into the CE chip, we were not able to detect insulin concentration concurrently with fluorescence monitoring. Instead, we collected fractions of the perfusate, FITC-insulin, and Ab by

using a perfusion chamber mixer device. We then collected the fractions into tube of droplets that was connected directly to the CE chip. To expand on this work, an electropherogram from the collection fractions will need to be performed.

2.8 References

- Abate, A.R., M., Pascaline, van Steijn, V., Wietz, D.A.: Experimental validation of plugging during drop formation in a T-junction. Lab on a Chip. 12:1516-1521, 2012.
- Fair, R.B.: Digital microfluidics: is a true lab-on-chip possible? Microfluidics and Nanofluidics. 3:245-281, 2007.
- Garstecki, P., Ganan-Calvo, A.M., Whitesides, G.M.: Formation of bubbles and droplets in microfluidic systems. Bulletin of the Polish Academy of Sciences Technical Sciences. 53:362-372, 2005.
- Gruessner, A.C., Sutherland, D.E.R.: Pancreas transplant outcomes for United States (US) and non-US cases as reported to the United Network for Organ Sharing (UNOS) and the International Pancreas Transplant Registry (IPTR) as of October. Clin. Transpl. 41-77, 2002.
- Hedeskov, C.J.: Mechanism of glucose induced insulin secretion. Physiol. Rev. 60:442-509, 1980.
- Inoue, K., Miyamoto, M.: Islet transplantation. J. Hepatobiliary Pancreat. Surg. 7:163-77, 2000.
- Keymeulen, B., Vandemeulebroucke, E., Ziegler, A.G., Mathieu, C., Kaufman, L., Hale, G., Gorus, F., Goldman, M., Walter, M., Candon, S., Schandene, L., Crenier, L., De Block, C., Seigneurin, J.M., De Pauw, P., Pierard, D., Weets, I., Rebello, P., Bird, P., Berrie, E., Frewin, M., Waldmann, H. Bach, J.F., Pipeleers, D., Chatenoud, L.: Insulin needs after CD3-antibody therapy in new-onset type 1 diabetes. New Engl. J. Med. 352:2598-2608, 2005.
- Lin, J.M., Sternesjo, J., Sandler, S., Bergsten, P.: Preserved pulsatile insulin release from prediabetic mouse islets. Endocrinology. 140:3999-4004, 1999.
- Maechler, P., Carobbio, S., Rubi, B.: In beta-cells, mitochondria integrate and generate metabolic signals controlling insulin secretion. Int. J. Biochem. Cell Biol. 38:696-709, 2006.
- Mohammed, J.S., Wang, Y., Harvart, T.A., Oberholzer, J., Eddington, D.T.: Microfluidic device for multimodal characterization of pancreatic islets. Lab on a Chip. 9:97-106, 2009.

- Okubo, Y., Shimada, A., Kanazawa, Y., Shigihara, T., Oikawa, Y. Imai, T., Miyazaki, J., Itoh, H.: Hyperplastic islets observed in “reversed” NOD mice treated without hematopoietic cells. Diabetes Res. Clin. Pract. 79:18-23, 2008.
- Robertson, R.P.: Islet transplantation as a treatment for diabetes-A work in progress. New Engl. J. Med. 350:694-705, 2004.
- Schultz, N.M., Huang, L., Kennedy, R.T.: Capillary electrophoresis-based immunoassay to determine insulin content and insulin secretion from single islets of Langerhans. Anal. Chem. 67:924-929, 1995.
- Shapiro, A.M.J., Lakey, J.R.T., Ryan, E.A., Korbitt, G.S., Toth, E., Warnock, G.L., Kneteman, N.M., Rajotte, N.M.: Islet transplantation in seven patients with type 1 diabetes mellitus using a glucocorticoid-free immunosuppressive regimen. New Engl. J. Med. 343:230–238, 2000.
- Song, H., Tice, J.D., Ismagilov, R.F.: A microfluidic system for controlling reaction networks in time. Angew. Chem. Int. Edit. 42:768-772, 2003.
- Tan, Y.C., Cristini, V., Lee, A.P.: Monodispersed microfluidic droplet generator by shear focusing microfluidic device. Sensors and Actuators B: Chemical. 114:350-356, 2006.
- Tao, L., Aspinwal, C.A., Kennedy, R.T.: On-line competitive immunoassay based on capillary electrophoresis applied to monitoring insulin secretion from single islets of Langerhans. Electrophoresis. 19:403-408, 1998.
- Thorsen, T., Roberts, R.W., Arnold, F.H., Quake, S.R.: Dynamic pattern formation in a vesicle-generating microfluidic device. Phys. Rev. Lett. 86:4163-4166, 2001.
- Tice, J. D., Song, H., Lyon, A. D., Ismagilov, R. F.: Formation of Droplets and Mixing in Multiphase Microfluidics at Low Values of the Reynolds and Capillary Numbers. Langmuir. 19:9127-9133, 2003.
- Xu, Y.: Tutorial: Capillary Electrophoresis. The Chemical Educator. 1, 1996.

Chapter 3: Series of tubes – A novel technique using silicone tubing for oxygen sensitive experiments

3.1 Abstract

In oxygen (O_2) sensitive experiments involving microfluidic devices, there is a need to eliminate costly, specialty O_2 tanks. To meet this need, highly O_2 permeable silicone tubing can be used to generate a variety of O_2 concentrations. By perfusing 0% O_2 into a variety of silicone tubing diameters and lengths, O_2 from ambient air diffuses across the wall of the tubes, changing the final gas concentration. A FOXY fiber optic oxygen probe was used to measure the final gas concentration. With silicone tube of 30 feet long and 1 inch diameter, the O_2 concentration at the end of tubing was ~14%. By decreasing the diameter of the tube to 1/2 inch, the O_2 concentration was ~8%. Using this technique to generate new gas concentrations, it can be combined with O_2 permeable microfluidic devices.

3.2 Introduction

Microfluidic technology allows for the precise control and manipulation of a variety of fluids and gases (Shamloo 2008, Oppegard 2010, Lo 2010, and Mohammed 2009). Most microfluidic experiments involving gases utilize oxygen (O_2) in the experiments (Oppegard 2010, Lo 2010, Rexius 2014). The devices for these experiments use O_2 sensitive membranes such as PDMS (Oppegard 2010) and cellulose (Su 2002). In many cases, a particular concentration of O_2 is needed to perform the experiment (Rexius 2014 and Mauleon 2012). Generally, in order to apply different concentrations of O_2 to the devices, a variety of O_2 gas tanks are required, which can be quite costly. To bypass this need, we propose a technique employing gas permeable silicone tubing.

At room temperature, silicone tubing is highly gas permeable. Silicone is made of mixed inorganic and organic polymers. The backbone of the polymer consists of chains

of silicon-oxygen (...-Si-O-Si-O-Si-...). The highly flexible –Si–O–Si– chains have “gaps” that allow for gas diffusion across the membrane (Zhang 2006). Silicone is highly permeable to O₂ with a permeability of 600 x 10⁻¹⁰ cm²/sec(cm-Hg) while having a nitrogen (N₂) permeability of 280 x 10⁻¹⁰ cm²/sec(cm-Hg). By infusing silicone tubing with 0% O₂ (or 100% N₂), we expect O₂ from ambient air to be able to permeate into the silicone tubing due to the higher permeability of O₂.

The flow, or flux, of mass through the membrane of the silicone tube can be modeled with Fick’s first law:

$$J = -D \frac{\partial c}{\partial x} \quad (3.1)$$

where J is the diffusion flux, D is diffusion coefficient, c is concentration of the permeate, and x is the thickness of the membrane. This equation tells us that the rate of transfer of a diffusing gas through a particular area is proportional to the concentration gradient (Zhang 2006). The amount of gas, or O₂, that diffuses across silicone tubing is dependent upon the thickness of the tube, as seen in equation 3.1. In addition, the amount of O₂ that diffuses into the silicone tube is dependent upon the area in which the O₂ has to diffuse across.

With this understanding, we will evaluate different diameters and lengths of silicone tubing, while maintaining the same wall thickness, to determine how, and if, O₂ from ambient air is able to diffuse across the wall and into the tube. If O₂ is able to diffuse into the silicone tube, we should discover a change of O₂ concentration at the outlet of the tubing. With a change of O₂ concentration, this technique could be used in combination with O₂ sensitive experiments, minimizing the need of costly gas tanks.

3.3 Materials and methods

3.3.1 Types of tubing

To determine how the permeability of silicone tubing can increase the concentration of 0% oxygen, a variety of lengths and diameters were tested. For calibration and control, tygon tubing was used. Majority of the tubing was purchase from Cole-Parmer and Harvard Apparatus. Table 1 shows the size and diameter of the tubing used. All tubing had a wall thickness of 1/32 inch.

<i>Type of Tubing</i>	<i>Internal Diameter (in)</i>	<i>Lengths tested (ft)</i>
<i>Tygon</i>	<i>1/16</i>	<i>1, 2.5, 5, 7.5, 10, 20, 30</i>
	<i>1/16</i>	<i>1, 2.5, 5, 7.5, 10, 20, 30</i>
	<i>1/8</i>	<i>1, 2.5, 5, 7.5, 10, 20, 30</i>
<i>Silicone</i>	<i>1/4</i>	<i>1, 2.5, 5, 7.5, 10, 20, 30</i>
	<i>1/2</i>	<i>1, 2.5, 5, 7.5, 10, 20, 30</i>
	<i>1</i>	<i>1, 2.5, 5, 7.5, 10, 20, 30</i>

Table 3.1. List of tubing and dimensions

3.3.2 Fabrication of 6-well insert

To validate that silicone tubing could be used for oxygen sensitive experiments, a 6-well hypoxic insert designed and validated by Oppegard (2010) was used, Figure 3.1. The insert consisted of 3 main sections: a PDMS membrane, a PDMS microchannel, and a PDMS pillar.

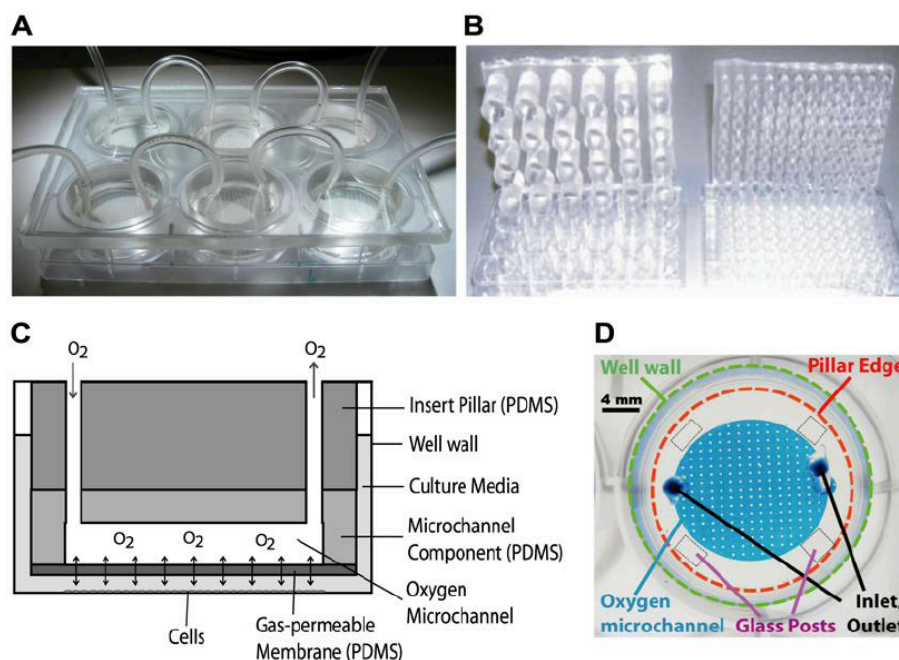


Figure 3.1. Schematic and images of 6-well insert. A) 6-well insert nestled into 6-well plate. B) Examples of 24 and 96-well inserts. C) Cross-sectional schematic of one pillar of the 6-well insert. Oxygen flows through the inlet and flows across the microchannels where it diffuses across a thin gas permeable PDMS membrane and dissolve into the culture media. D) Top view image of oxygen microchannel. (Reprinted from Oppegard 2010)

The microchannel, Figure 3.1d, was fabricated using standard photolithography methods. SU-8 2150 was spun at 500 rpm for 10 seconds and 3000 rpm for 30 seconds onto a silicon wafer to achieve a height of 400 μm . The silicon wafer was then baked at 65° C for 10 minutes, 95° C for 90 minutes, and cooled to room temperature. A photomask of the microchannel design was laid on top of the wafer and exposed to 500 mJ/cm^2 of UV light to polymerize the exposed areas. Afterwards, the silicon wafer was placed onto a hotplate at 65° C for 5 minutes and 95° C for 25 minutes. Once the post exposure bake was completed, the silicon wafer was placed into SU-8 developer atop a shaker for about 20 minutes. 5 g of premixed PDMS was poured and cured unto the microchannel master to obtain a desired height of 1 cm. Each master had 3 microchannels. For a 6-well insert, PDMS had to be casted unto the master once more.

A Delran mold designed and previously discussed by Opegard was used to fabricate the 6-well pillar insert. Each well mold had a height of 16 mm and a diameter of 31 mm, Figure 3.1. Once the mold was prepared, 130 g of PDMS was mixed, poured, and baked overnight at 75° C to ensure in uniform baking.

For membrane fabrication, a previously used silicon wafer free of SU-8/PDMS was thoroughly cleaned with isopropanol (IPA), acetone, and Kim wipes. A premixed PDMS mixture was poured onto the silicon wafer and spun at 500 rpm for 10 seconds and 800 rpm for 30 seconds; this spin speed ensured in a membrane thickness of 100 µm. After spinning, the wafer was baked at 65° C for 2 hours. A circle, the size of the microchannel, was cut into the membrane. 6 of these circles were cut out of the wafer for bonding to the microchannels.

The bonding process of the 6-well insert device involved several steps. The microchannels were bonded to the PDMS 6-well pillar, once it was removed from the Delran mold, by thoroughly cleaning and plasma treating their surfaces. The newly bonded pillar was baked on a hot plate for 20 minutes at 120 ° C to ensure the pieces are securely bonded. Once cooled, two 11 gauges punches were bored into each microchannel/pillar combo. The microchannels and membranes were then thoroughly cleaned, plasma treated, and bonded together. The device was then placed in an oven at 120° C for 1 hour.

After baking, each pillar was tested for leaks. This testing was done by running air through each well with the device was submerged under water.

3.3.3 Design of oxygen perfusion chamber

Due to limitations with the 6-well insert device, a single perfusion chamber was also designed. The perfusion chamber is a 3 layer PDMS device. It contains a

microchannel, the same as in the 6-well insert, a membrane, and a 3 mm thick PDMS chamber, Figure 3.2. The perfusion chamber was designed to have the gas flow within the microchannels, through the membrane, and into ambient air, or water sitting in the chamber.

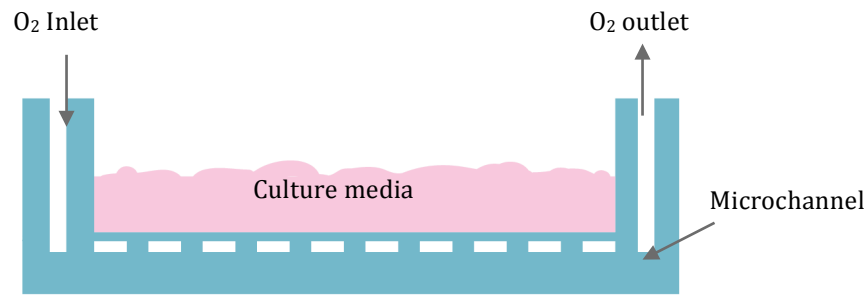


Figure 3.2. Schematic of oxygen perfusion chamber

3.3.4 Fabrication of oxygen perfusion chamber

The oxygen perfusion chamber was designed using standard photolithography methods. A microchannel master was fabricated as described in section 4.3.3. In a 4 inch petri dish, 75 g of 10:1 PDMS was poured to obtain a height of 3 mm once cured. A 100 μm membrane was fabricated as previously described in 4.3.3.

The 3 mm thick PDMS was removed from the petri dish and cut into several 31 mm circular discs. The discs were then punched with a 1 inch diameter puncher to remove the center of the disc, creating the chamber part of the device. The disc was then bonded to the membrane wafer using a corona treater and then baked at 120° C. The membrane and disc combo was removed from the wafer and two 11 gauge holes were punched from the membrane through the disc. After this was done, the membrane was bonded to the microchannel using a corona treater and baked at 120° C for 15 minutes.

As previously described with the 6-well insert device a leak test was performed by blowing air through the perfusion chamber while submerged underwater.

3.3.5 Fabrication of PtOEPK

For oxygen characterization of the silicone tubing with the 6-well insert device, platinum(II) octaethylporphine ketone (PtOEPK, Frontier Scientific) was placed at the bottom of each well. The intensity response of the PtOEPK sensor was monitored to the changing oxygen concentrations, which allowed for the determination of the oxygen concentration within the 6-well plate.

In order to fabricate the PtOEPK sensors, a mixture of 35% (w/w) polystyrene(PS)/toluene was made by mixing the two together on a shaker for 24 hours. PtOEPK powder was added to the PS mixture at 1 mg/ml and put on a shaker for 24 hours. After, the solution was poured onto a glass slide and spun at 1000 rpm. The slide was placed in a fume hood, covered with aluminum foil, and left overnight so the toluene evaporated. This process results in the PtOEPK sensor embedded in PS.

3.3.6 Calibration for tube analysis

For calibration, a 6 inch long 1/16 inch ID tygon tube was used. 0%, 10%, and 21% O₂ were flowed through the tube at a flow rate of 13 mL/min. Each concentration flowed for 5 minutes before it was recorded with the NeoFox software. This was done at the beginning and end of each tube measurement. The calibration results were averaged and compared to final data collected from the NeoFox software.

3.3.7 Experimental setup for tube analysis

To determine the change of oxygen concentration from the beginning to the end of a tube, a FOXY fiber optic oxygen probe (Ocean Optics, AL300) was used, Figure 3.3. The end of each tube was enclosed with a connector to allow for minimal introduction of

outside air. The probe was inserted through the connector and aligned in the middle of the tubing. The FOXY probe outputted readings to a NeoFox fluorimeter that induces fluorescence and examines the emission spectrum. It communicated with Ocean Optics software and displayed the oxygen concentration on the screen. The inlet of each tube was connected to a rotometer, which in turn was connected to a gas tank. The flow rate of 13 mL/min was used for each tube. After the start of each experiment, recordings immediately began and lasted for 30 minutes ensuring the concentration equilibrated. The last minute each recording was averaged to give the final result of oxygen concentration.

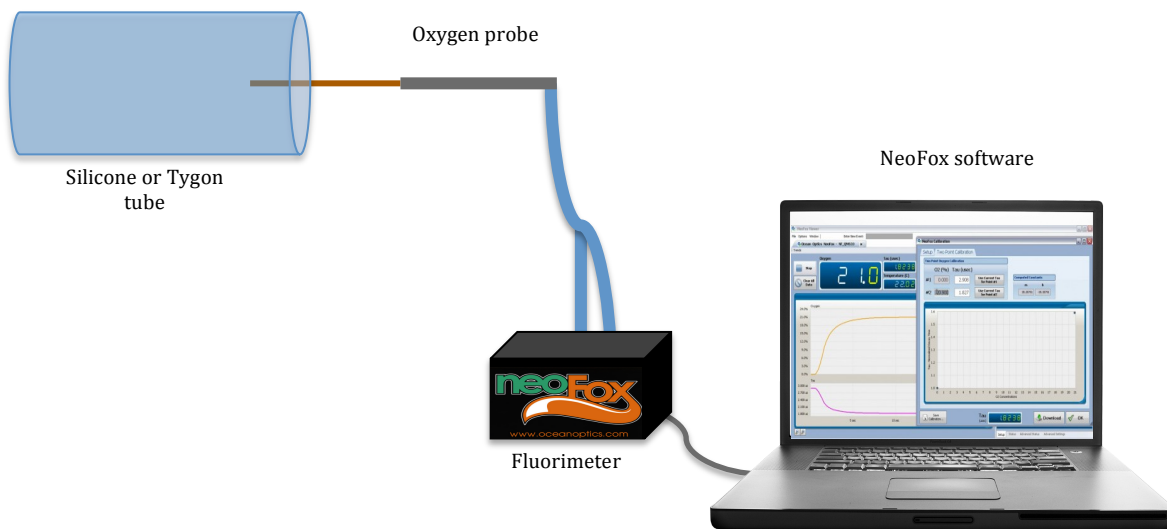


Figure 3.3. Experimental setup for tube analysis with oxygen sensing probe. Not drawn to scale.

3.3.8 Calibration for 6-well insert

The PtEOPK of each well was calibrated by flowing 0%, 10%, and 21% O₂ through each individual well insert. A thin layer of water was added to each well. Images were taken on an inverted microscope using Metamorph software. After 10 minutes of constant gas flow, 10 images of each well and at each concentration were taken. The

fluorescent intensities of each image were averaged and determined for the respective concentration.

3.3.9 Experimental setup for 6-well insert

The outlet of each tube was connected to an inlet of the 6-well insert device. 0% O₂ flowed through the tubes at 13 mL/min. PtEOPK was placed at the bottom of each well. Using the moving stage of an inverted microscope, the fluorescence change of the PtEOPK in each well was recorded. This experiment lasted one hour with images taken every 30 seconds. The last minute of images was averaged together to determine the final concentration of the well inserts. This was then compared to the calibration data and normalized.

3.3.10 Calibration of perfusion chamber using PtEOPK

Calibration methods were similar to that described in section 4.3.8. Only one chamber was calibrated at a time.

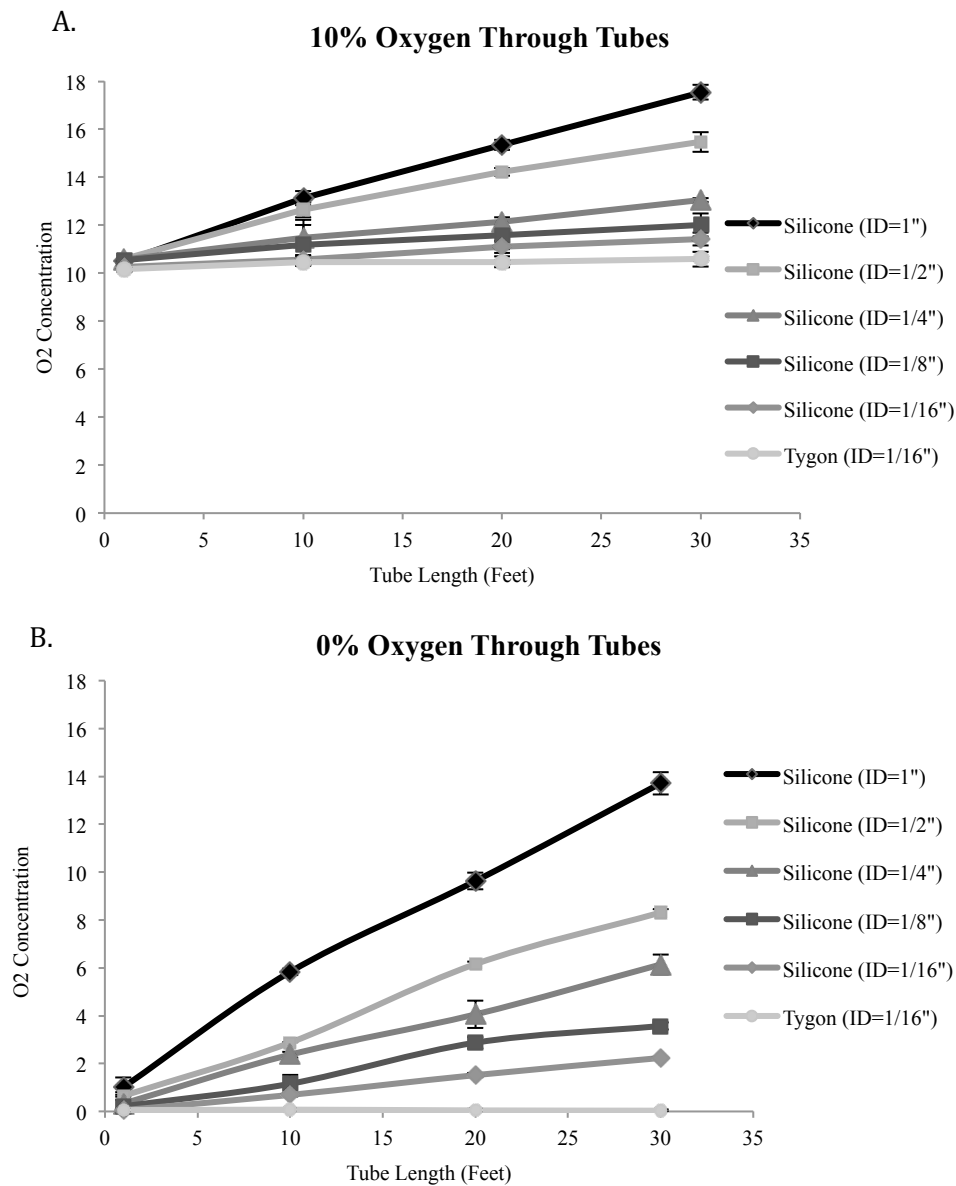
3.3.11 Experimental setup of perfusion chamber using PtEOPK

The outlet of the tube being test was connected to the inlet of the perfusion chamber. A small PtEOPK sensor was placed on top of the device membrane and 2 mL of water was added to the chamber to represent media. 0% O₂ flowed from the gas tank through the tubing and to the device at 13 mL/min. The outlet of the perfusion chamber was connected to a tygon tube inserted in water to validate gas flow through the device; this was evident with the formation of bubbles in the water. Intensity images were taken of the sensor every 30 seconds for 1 hour. After this was done, the last minute of the intensity values were averaged, compared, and normalized to the calibrated results.

3.4 Results

3.4.1 Results of tube analysis

The final oxygen concentration from varying tubing lengths and diameters with 0% and 10% O₂ flowing through was determined. The results obtained are shown in Figure 3.4.



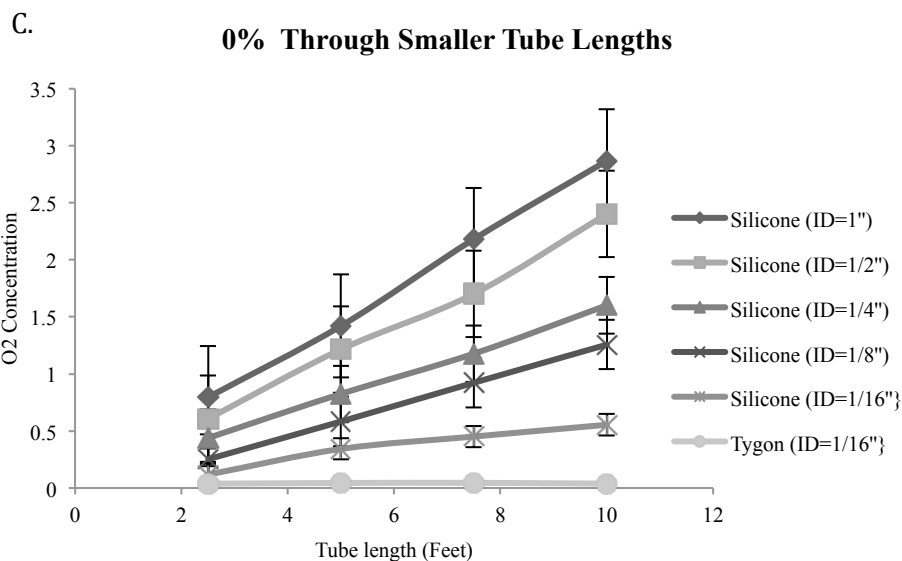


Figure 3.4. Oxygen concentration at different lengths and diameters of silicone and tygon tubing. A) 10% O₂ flowing through silicone and tygon tubing at 1 ft, 10 ft, 20 ft, and 30 ft. B) 0% O₂ flowing through silicone and tygon tubing at 1 ft, 10 ft, 20 ft, and 30 ft. C) 0% O₂ flowing through silicone and tygon tubing at 2.5 ft, 5 ft, 7.5 ft, and 10 ft. N=3 for all graphs.

3.4.2 Results of 6-well insert

A 10 ft, 1/2 inch silicone tube was connected to the 6-well insert. After the 4 hours, it was quickly determined that there was little to no change in oxygen concentration across the PDMS membrane for n=1, Table 3.2.

Well	O ₂ concentration
1	19.43755
2	18.67745
3	22.07861
4	20.09743
5	20.33193
6	20.59661

Table 3.2. Oxygen concentration obtained from n=1 of 6-well insert with 10 ft, 1/2 inch diameter silicone tube.

3.4.3 Results of perfusion chamber

Experiment ran for 4 hours with 10 ft, 1/2 inch diameter silicone tube, an oxygen concentration of 9.76% was obtained for n=1.

3.5 Discussion

3.5.1 Tube analysis

The oxygen concentration data showed that the concentration does change due to the permeability of silicone tubing. With 10% O₂ flowing through silicone tubing 30 ft long with a diameter of 1 inch, a concentration of about 18% was obtained. With 0% O₂ flowing through the same silicone tube, a concentration of about 14% was obtained. For both initial gas flows, the concentration maintained constant for tygon tubing, the control, proving that tygon is gas impermeable. The final concentration increased linearly as the diameter and tube length increased.

It was then decided to find the final O₂ with smaller tubing lengths, Figure 3.4c, since the smaller lengths would be easier to maneuver during experiments with microfluidic devices. From Figure 3.4b, we estimated O₂ concentration for the 1 inch, 10 ft silicone tubing to be about 6% and that the concentration would decrease linearly as the tube length decreased. However, when the concentration was reevaluated at 1 inch, 10 ft, it was found that the concentration was about 3%. O₂ concentration varied from Figure 3.4b and 3.4c. This change may be due to variations from the FOXY probe, gas flow rates, or pressure variations within the outlet of the tubing.

Even though the O₂ concentrations for each tube in Figure 3.4c is much lower than expected, the O₂ levels are higher than the inputted O₂ concentration of 0%. This concentration change within the tubing shows that ambient air is able to diffuse into the silicone tube.

3.5.2 6-well insert device

The inlet of the 6-well insert was connected to a 10 ft, 1/2 inch diameter silicone tube. From Figure 3.4c, it was estimated that the O₂ concentration of each well would be 2.5%. However, Table 3.2 shows that the O₂ concentration of each well did not decrease. The first two wells had an O₂ concentration slightly lower than 21%, but the change was insignificant. All other wells maintained a concentration within 1% of normoxic conditions. The lack of concentration change may be due to low flow rate from the silicone tubing. Backpressure caused by the 6-well insert may have also affected diffusion across the PDMS membrane. The pressure from the insert may have caused the gas to flow much slower than expected. Since after 4 hours there is a slight decrease of O₂ concentration in the first two wells, it is possible that the concentration may decrease if the experiment is left to run longer.

3.5.3 Perfusion chamber

The perfusion chamber was connected to a 10 ft, 1/2 inch diameter silicone tube with 0% O₂ flowing at a rate of 13 mL/min. After 4 hours, it was found that the O₂ concentration in the perfusion chamber decreased from 21% to a concentration of 9.76%. This is a good indication that ambient air diffused into the silicone tube while 0% O₂ flowed into the tube. However, this concentration is much higher than expected. From Figure 3.4c, it was estimated that the concentration across the perfusion chamber membrane would be 2.5%. If the experiment was left to run longer, it is possible that the concentration may continue to decrease. It is difficult to determine the true cause of the concentration differences between using the silicone tube standalone or with a microfluidic device with just one experiment. More experiments with the same tube and smaller tubing would need to be examined.

3.6 Future directions

For future experiments with microfluidic devices, it may be beneficial to run experiments much longer than 4 hours. It would also be necessary to reexamine the final concentration of each tube by using pressure flow instead of the rotometers. The flow rate varies between different gasses when using a rotometer. Steps were taken for each experiment to verify that the same flow rate was used, however, errors may have occurred. In addition, when measuring the concentration within a microfluidic device, the concentration being outputted by the silicone tubing should also be measured.

Modifications to the current setup would need to be made in order to insert a FOXY probe directly into the end of tube while simultaneously providing gas to the microfluidic device. Additionally, tygon tubing with the same diameters as silicone tubing should also be examined to determine the change in O₂ concentration is strictly due to the diffusion of concentration across the silicone tube and not due to pressure differences in the larger diameter.

3.7 Conclusions

In this research, we were able to demonstrate gas diffusion in gas permeable silicone tubes. By varying the diameter and length of the tubes, we were able to generate a variety of O₂ concentrations by infusing 0% O₂ into the tubes. We connected the outlet of a 2.5 inch diameter, 10ft tube to a 6-well insert. We were unable to generate the same concentration across the membrane of the 6-well insert. We next connected the same tube to a perfusion chamber device and found that the concentration across the membrane decreased from 21% to 9.46%. This shows that ambient air is diffusing across the silicone tubing and into the microfluidic device. Further analysis needs to be performed to better understand the diffusion of ambient air across the silicone tubes. In addition, experiments

with the microfluidic devices need to be performed longer to allow for better equilibration of the gas diffusing into the devices.

3.8 References

- Lo, J.F., Sinkala, E., Eddington, D.T.: Oxygen gradients for open well cellular cultures *via* microfluidic substrates. Lab on a Chip. 10:2394-2401, 2010.
- Mauleon, G., Fall, C.P., Eddington, D.T.: Precise spatial and temporal control of oxygen within *in vitro* brain slices via microfluidic gas channels. PloS One. 7: e43309, 2012.
- Mohammed, J.S., Wang, Y., Harvart, T.A., Oberholzer, J., Eddington, D.T.: Microfluidic device for multimodal characterization of pancreatic islets. Lab on a Chip. 9:97-106, 2009.
- Oppegard, S.C., Blake, A.J., Williams, J.C., Eddington, D.T.: Precise control over the oxygen conditions within the Boyden chamber using a microfabricated insert. Lab Chip. 10:2366-2373, 2010.
- Rexius-Hall, M.L., Mauleon, G., Malik, A.B., Rehman, J., Eddington, D.T.: Microfluidic platform generates oxygen landscapes for localized hypoxic activation. Lab on a Chip. 14:4688-4695, 2014.
- Shamloo, A., Ma, N., Poo, M., Sohm, L.L., Heilshorn, S.C.: Endothelial cell polarization and chemotaxis in a microfluidic device. Lab on a Chip. 8:1292-1299, 2008.
- Su, Y.C., Lin, L.: A water-powered micro drug delivery system. Journal of Microelectromechanical Systems. 13:75-82, 2001.
- Zhang, H., Cloud, A.: The permeability characteristics of silicone rubber. Society for the Advancement of Material and Process Engineering. 2006.

VITA

ELIZABETH FERRAZ

- Education**
- University of Illinois at Chicago, IL**
Master of Science in Bioengineering, Pending Thesis defense
Advisor: David Eddington
Thesis: Microfluidic Applications For The Study Of Pancreatic Islets, Gradient Formation, And Gas Diffusion
- University of Illinois at Chicago, IL**
Bachelor of Science in Bioengineering, August 2010
Concentration in Cells and Tissues Engineering
Minor in Mechanical Engineering
- Research Experience**
- 06/10-Present **Biological Microsystems Laboratory, University of Illinois at Chicago, IL**
Graduate Research Assistant, Master Thesis Project
- Developing a droplet microfluidic device that combines stimulated islet cell perfusate, fluorescein isothiocyanate(FITC)-labeled insulin, and anti-insulin antibodies into a droplet that can later be analyzed by a capillary electrophoresis device developed by our University of Michigan collaborators
- 01/10-08/10 **Biological Microsystems Laboratory, University of Illinois at Chicago, IL**
Undergraduate Research Assistant
- Assisted in the design and development of a microfluidic yeast trapping device for the study of yeast chemotropism
 - Assisted in experiments validating gradient formation within the yeast trapping device
 - Cultured yeast for experimental use
- 08/09-08/10 **Senior Design Project – Identia-a-pill, University of Illinois at Chicago, IL**
Undergraduate Researcher
- Developed a device capable of identifying pills through use of a CCD and Matlab program replacing the need of a Physician's Desk Reference
 - Developed a Matlab program for image analysis of up to 10 individual pills based on characteristics

- 08/09-05/10 **Biomedical Engineering Society, University of Illinois at Chicago, IL**
Head of high school outreach committee
- Coordinated group meetings
 - Supervised creation of power point presentation
 - Collaborated with different research labs to create videos of labs
- Engineering World Health*
- Coordinated group meetings
 - Supervised construction of electrosurgery tester units
 - Educated members on basic soldering skills

Work Experience

- 08/10-05/11 **University of Illinois at Chicago, IL**
Teaching Assistant
- Tutored and assisted students with assignments and course concepts in two courses: Biomaterials and Microfluidics
 - Graded assignments
 - Lectured and developed laboratory coursework for Microfluidics
- 08/03-08/10 **Arlington Heights Animal Hospital, Arlington Heights, IL**
Kennel Attendant and Veterinary Assistant
- Maintained a clean and healthy environment for animals, clients, and employees
 - Responsible for opening and closing the facility
 - Provided care for all animals during boarding, hospitalization, and after surgeries
 - Assisted doctors with check-ups, restraint, and x-rays
 - Administered medication and subcutaneous fluids
 - Bathed animals
 - Assisted in euthanization when necessary
 - Trained employees

Skills

- Extensive technical writing experience.
- Experience scientific presenter.
- Experience in training new staff
- Technical expertise in bioengineering and life science methodologies, including cell and tissue culture, enzyme-linked immuno-sandwich assay analysis, fluorescence microscopy and immunocytochemistry, mice islet isolation, soldering techniques, and microfluidic device fabrication (soft lithography).
- Proficient at a wide variety of software packages, including the Microsoft Office suite, AutoCAD, SolidWorks, ProE, COMSOL, Matlab, NeoFox, C++, MetaMorph, and MetaFluor.

Awards

- UIC President's Award Program, 2005-2007
- Chancellor's Student Service Award, 2010

Conferences

- Society for Laboratory Automation and Screening – San Diego, IL (January 2014)
Title: "On Chip Immunoassay for Pancreatic Islets"
- University of Illinois at Chicago Engineering Expo – Chicago, IL (April 2010)
Title: "Ident-a-Pill: Pill Identification System"
- University of Illinois at Chicago Research Forum – Chicago, IL (April 2010)
Title: "Soft Lithography for Rapid Prototyping of a Three Layer Microfluidic Device"